Received: 20 July 2020 | Revised: 13 October 2020 | Accepted: 27 November 2020

DOI: 10.1002/stc.2683

WILEY

RESEARCH ARTICLE

Dissipative steel exoskeletons for the seismic control of reinforced concrete framed buildings

Fabio Mazza

Dipartimento di Ingegneria Civile, Università della Calabria, Rende, Italy

Correspondence
Fabio Mazza, Dipartimento di Ingegneria Civile, Università della Calabria, Rende, Cosenza, Italy.
Email: fabio.mazza@unical.it

Funding information
Re.L.U.I.S.

Summary

The insertion of steel bracing systems equipped with dissipative devices is a widely used technique for the seismic retrofitting of reinforced concrete (r.c.) framed buildings; yet, few attempts have been made so far to construct an external arrangement in the form of a double skin. The dissipative exoskeleton (DEX) appears convenient from energetic and functional points of view. It eliminates the indirect costs associated with downtime during retrofitting and cuts out the unwanted effects to the existing structure that commonly arise with the dissipative endoskeleton. This paper provides a DEX sizing procedure through use of overdamped elastic response spectra, which could prove a valuable tool for practitioners. The DEX is designed on the assumption of a rigid coupling with the existing structure, making a distinction between mass and stiffness properties of the steel exoskeleton and added damping of the dissipative bracing system. Concentrically braced chevron frames with pinned joints and damped bracing systems incorporating fluid viscous dampers (FVDs) are considered. Elastic-linear behaviour of steel frame members and nonlinear pure viscous dashpot for FVDs, with a storey-shear proportional distribution, are hypothesised. The retrofitting of a six-storey r.c. framed structure, representative of the Italian residential buildings designed for moderate seismic loads during the 1990s, is to be simulated in a high risk-seismic region. Three external arrangements of DEX are selected: parallel (DEX.Pa) and perpendicular (DEX.Pe) to all façades of the existing building and a mixed solution (DEX.Mi) with both parallel and perpendicular disposition placed along the shorter façades without apertures. Nonlinear structural models of the original (F) and coupled (DEXF) structures are developed in OpenSEES, considering ductile and brittle failure modes of r.c. elements and joints. The seismic analyses not only confirm the effectiveness of the proposed DEX design but also provide insights into the strength and weaknesses of the examined configurations.

KEYWORDS

design procedure, dissipative steel exoskeletons, nonlinear fluid viscous dampers, r.c. framed buildings, seismic retrofitting

1 | INTRODUCTION

The use of a dissipative endoskeleton (DEN), constituted of steel supporting braces connecting adjacent storeys and equipped with devices dissipating energy by means of different mechanisms (e.g., metallic yielding, friction sliding, fluid orificing, viscoelastic deformation, and phase transformation of metals), is an effective and widely used technology for the retrofitting of buildings as it offers certain advantages (e.g., ease of inspection and replacement and low maintenance costs) in comparison to traditional solutions.[1–7] However, the insertion of dissipative braces in structures built in line with former seismic codes can induce significant changes in their collapse mechanism with a notable increase in the axial load transmitted to columns and foundations,[8] requiring local strengthening and great care and attention when connecting joints to the original frame.[9] A number of other potential downsides are worth mentioning. The indirect costs associated with the temporary relocation of residents and service interruption during installation can be considerable; the retrofit itself can be invasive and compromise building usage, and application along the façade can interfere with existing masonry infills. In view of the above, alternative strategies using external dampers can be used as a way to overcome these problems.

One option exploits the horizontal displacement between the existing structure and external reaction structures (e.g., fixed r.c. walls and steel towers), which are connected by dissipative links at the floor levels.[9–11] The advantage of retrofitting from outside the structure is that interference with structural and nonstructural components inside the building can be avoided. However, the relative displacement caused by the added damping depends to a great extent on the properties of the adjacent structures,[11] so local strengthening of the existing slabs connected to the dampers may also be required.[10] Another alternative is the use of external post-tensioned walls[12–17] and steel braced towers,[18,19] centrally pinned at the foundation to impose uniform interstorey drift along the height of the frame. It should be noted that the self-weight of pinned rocking systems acts against stability, leading to permanent displacement unlike stepping rocking wall able to re-centre because of gravity.[20] Nevertheless, these solutions are still rarely used presumably for their complexity and lack of practical design procedures.[21] The dissipative exoskeleton (DEX), an external steel framed structure equipped with a damped bracing system and rigidly coupled to the existing building but with its own foundation, is suggested by seismic codes.[22] It provides a structural solution that can also combine functional and energetic issues while reducing downtime losses during the retrofitting process.[23–27] The added damping is activated by the relative displacements between adjacent floors of the DEX, whose dynamic properties are not necessarily very different from those of the existing structure.

In the present paper, external solutions for the seismic retrofitting of reinforced concrete (r.c.) framed buildings via EX dissipative structures are examined. The proposal consists of a sizing procedure of the DEX able to provide a useful tool for practitioners, by making distinction between mass, stiffness and strength properties of the steel EX and added damping of the dissipative bracing system. Fluid viscous dampers (FVDs) are selected because they do not contribute extra stiffness to the original structure, contrary to other types of devices that also apply lateral stiffness. Specifically, an iterative procedure with two nested loop cycles is implemented that, for an assigned value of the supplemental damping, evaluates additional stiffness (interior loop) and mass (exterior loop) of the DEX. An elastic-linear behaviour is hypothesised for the external concentric steel bracing system with chevron-pattern scheme, which is designed to prevent yielding in tension and buckling in compression of all members, while a nonlinear viscous response[28] is assumed for the chevron damped bracing system with FVDs inserted in the EX. Among the many design procedures for optimising vertical distribution of the FVDs,[29] a simplified methodology proportional to the storey shear[30] is preferred for an initial evaluation of their effectiveness and reliability. This is based on the reduced efficiency of the FVDs at the upper storey, where a decrease of the interstorey velocity is generally observed.

In the subsequent sections, the proposed design procedure is applied for the seismic retrofitting of a six-storey archetype in L'Aquila (Italy), representative of many r.c. buildings designed for moderate seismic loads prior to the 2008–2018 code changes.[31] The building is regular in plan with five longitudinal bays (i.e., main fronts corresponding to the north- and south-facing façades) and three bays in the transversal one (i.e., east- and west-facing façades without apertures). Interventions with DEXs are designed at the life-safety (LS) limit state, considering three alternatives: (i) parallel disposition running around all four façades (DEX.Pa), with a distance from the existing structure set to suit the new foundation and to allow the opening of windows; (ii) perpendicular disposition running around all four façades (DEX.Pe), with a floor slab defining new spaces increasing the well-being of the inhabitants along sides with north and south exposure; (iii) parallel–perpendicular mixed disposition (DEX.Mi), as an enlargement on the eastern and western sides only where energy saving measures could be added. Nonlinear static analysis using the software OpenSEES[32] is preliminarily carried out, to investigate the seismic vulnerability of the existing building. R.c. frame

members are modelled with lumped plasticity elements, with flexure- or shear-controlled moment–chord rotation at critical end sections,[33,34] while the shear behaviour of the beam-column joints is modelled by means of a scissor model.[35,36] In order to demonstrate effectiveness of the retrofitting interventions, nonlinear dynamic analyses of the bare (F) and coupled (DEXF) structures are carried out considering records scaled in line with a high-risk seismic region.

2 | PROPOSAL OF A DESIGN PROCEDURE FOR A DEX

2.1 | Approach

A design procedure of DEX systems incorporating nonlinear FVDs is implemented in this study, which focuses on displacement as the key sizing parameter and employs overdamped elastic response spectra. The procedure is a reformulated version of an approach recently derived for DEN systems,[37,38] conceived in such way as to make a clear distinction between the design of a steel EX (i.e., mass, stiffness and strength) and a dissipative bracing system (i.e., added damping) and an extension including nonlinear FVDs. The distinctive properties of the nonlinear FVD make it attractive for DEX systems: that is, negligible stiffening effect[39] and limitation of the transmitted force in the case of a marked increase of velocity.[40] By referring to two coupled equivalent single-degree-of-freedom (SDOF) systems shown in Figure 1, representing the original frame (F, black line) with an infinitely rigid but nondissipative connection to a DEX (blue line), relevant design parameters are mass and stiffness ratios.

$$\alpha_m = \frac{m_{e,DEX}}{m_{e,F}};\ \alpha_K = \frac{K_{e,DEX}}{K_{e,F}} \tag{1ab}$$

and uncoupled equivalent damping ratios ξ_F and ξ_{DEX}. Equivalent mass of the SDOF system representing the original frame can be evaluated by multiplying the first-mode (horizontal) components (ϕ_1, ϕ_2, ..., ϕ_n) by the corresponding floor masses ($m_{1,F}$, $m_{2,F}$, ..., $m_{n,F}$)

$$m_{e,F} = \sum_{i=1}^{n} (m_{i,F} \cdot \phi_i),\ \ (\phi_n = 1) \tag{2}$$

while equivalent (secant) stiffness depends on base shear ($V^*_{p,F}$) at the performance displacement (d^*_p)

$$K_{e,F} = \frac{V^*_{p,F}}{d^*_p} \tag{3}$$

resulting from the nonlinear static analysis of the original structure. A double iteration process is required because for an assigned value of ξ_{DEX} and known value of ξ_F, both corresponding to the assigned displacement demand d^*_p, the corresponding coupled total damping (ξ_{DEXF}) is function of the unknown stiffness ratio α_K, which, in turn, depends on the unknown mass ratio α_m. Selection of design values for the stiffness (e.g., α_K = 1–10) and mass (e.g., α_m = 0.01–0.30) ratios depends on structural (i.e., displacement demand) and functional (e.g., additional space in front of the building façades) requirements.

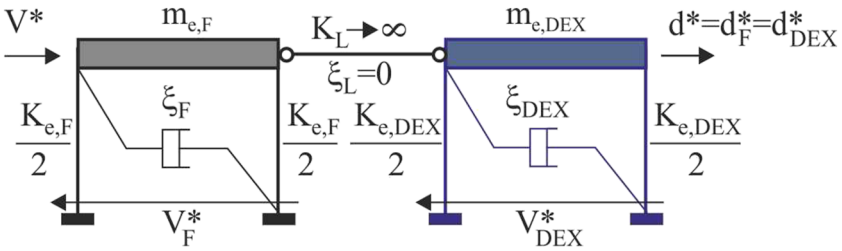

FIGURE 1 DEXF system as coupling of two equivalent SDOF systems

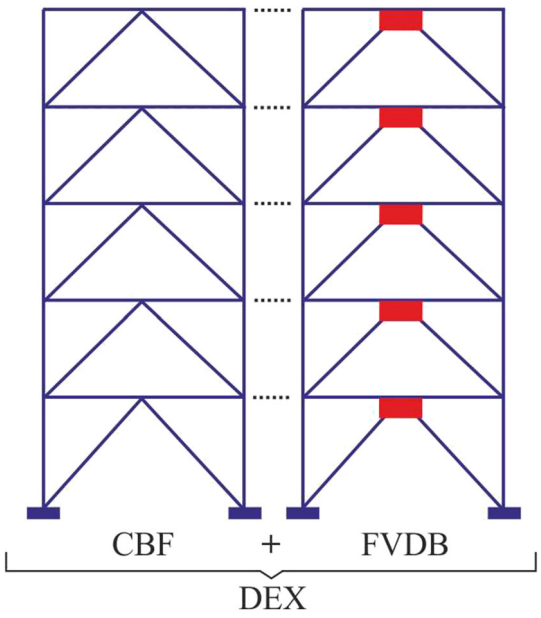

FIGURE 2 DEX system as coupling of CBFs and FVDBs

A concentrically braced frame (CBF) can be selected as steel EX that proves to be more cost-effective than the moment resisting frame, with beams and columns pinned at the end sections and chevron braces (Figure 2), to accommodate a wide range of architectural elements (such as doors and windows).

2.2 | Pros and cons of in-plan configurations of the DEX

The DEXs provide the opportunity for an energetic retrofit of the building envelope and are characterised by complete reversibility but compared to DENs not only the dissipative bracing system but also the new steel EX needs to be designed. Three typological choices of DEX are possible depending on the distributive (e.g., available space and compatibility with the architectural layout of the building) and energetic (e.g., thermal losses) features along the perimeter: parallel (DEX.Pa, Figure 3a) and perpendicular (DEX.Pe, Figure 3b) positioned to the façades to which it is connected through standard shear and axial links, respectively; mixed DEX (DEX.Mi, Figure 3c), where DEX.Pa and DEX.Pe are placed on the same façade. Diagonal steel members serve as links between DEXs.Pe of adjacent façades (Figure 3b), while internally (Figure 3b) and externally (Figure 3b,c) additional links parallel to the façades covered by DEXs.Pe and DEXs.Mi are placed for the purpose of attaining a spatial truss structure. It should be noted that DEX.Pa (Figure 3a) and DEX.Mi (Figure 3c) offer the possibility of perimetral shear links in addition to the nodal connection. Moreover,

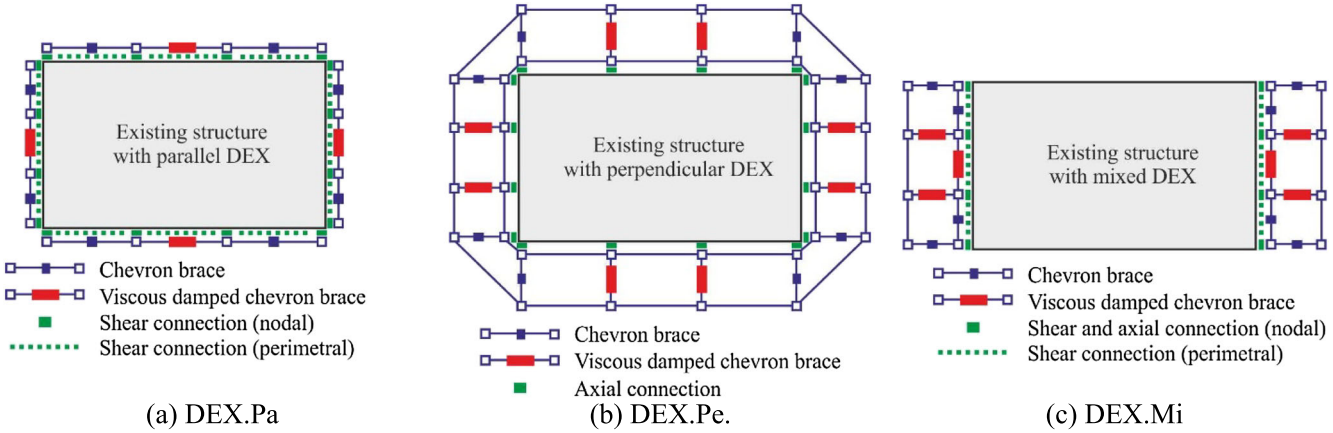

FIGURE 3 In-plan configurations of the dissipative exoskeleton (DEX)

DE.Pa always provides additional torsional stiffness to the original scheme, while arrangement of the DEX.Pe requires special attention to prevent a torsionally flexible system that may arise for the internal positions along the perimeter. A high degree of redundancy of the shear connection is obtained with DEX.Pa, exploiting the perimetral beams parallel to the DEX at each floor level, while only the axial connection with beam-column joints is possible for DEX.Pe. On the other hand, the added spatiality in the façades resulting from DEX.Pe allows the creation of new housing space, partially or totally covering the retrofitting costs by means of the increased real estate value, upgrades vertical accessibility (e.g., stairwells and lifts) as well as horizontal private or collective circulation (e.g., balconies and living spaces). However, the increased useful space provided by DEX.Pe corresponds to a non-negligible additional mass of the EX structure compared to the total mass of the building, thereby inducing seismic loads higher than those corresponding to the DEX.Pa arrangement. As this last solution supports gravity loads due to their self-weight only, large overturning moments induced by the horizontal seismic loads may lead to tensile axial force in its foundation.

2.3 | Displacement-based design procedure of the DEX

A four-step double-iteration design procedure of the DEX is proposed (Figure 4), whose design parameters are: target performance displacement evaluated through nonlinear static analysis of the existing structure; properties of the nonlinear FVDs, in terms of maximum equivalent viscous damping ratio ($\xi_{v,DB0}$) and velocity exponent (β); seismic loads. On the other hand, final unknown parameters are mass, stiffness and strength properties of the steel EX (e.g., CBF) and damping constant of the nonlinear velocity-dependent dampers (e.g., FVDs).

As depicted in the flowchart, the design procedure requires internal (step 3) and external (steps 3 and 4) iteration loops related to the stiffness ($\alpha_k^{(..)}$) and mass ($\alpha_m^{(..)}$) ratios, respectively. An initial approximation of these ratios is

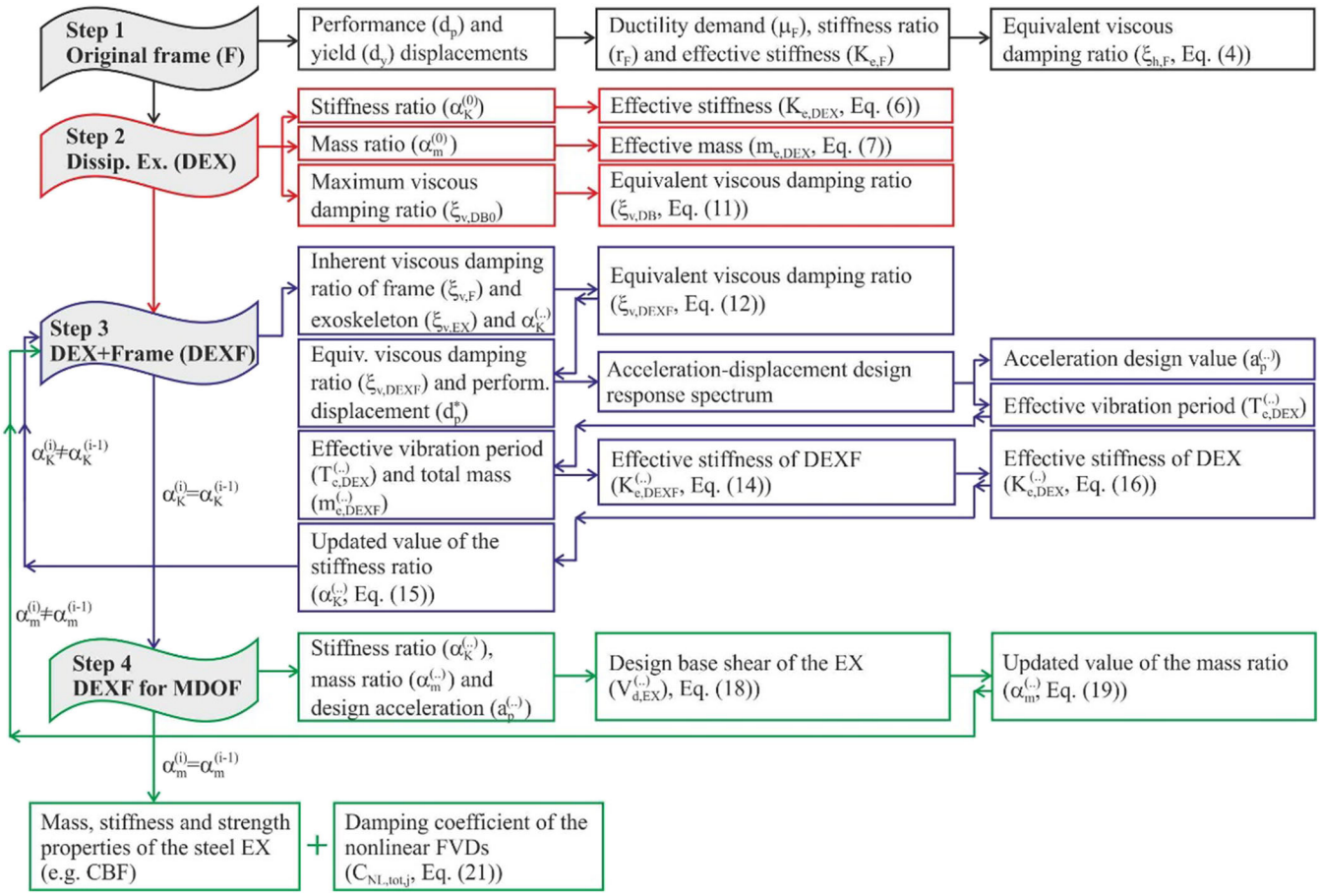

FIGURE 4 Flowchart of the displacement-based design procedure of the DEX

assigned in step 2 (i.e., $\alpha_k^{(0)}$ and $\alpha_m^{(0)}$) and then a sequence of iteration loops is performed until convergence to the correct values is attained (i.e., $\alpha_k^{(i)} \approx \alpha_k^{(i-1)}$ and $\alpha_m^{(i)} \approx \alpha_m^{(i-1)}$). Steps of the proposed design procedure are discussed below.

Step 1. Properties of the SDOF system equivalent to the original frame (F)

Black boxes in Figure 4 describe step 1, starting from the base shear (V_F) versus roof-storey displacement (d) capacity curve of the original framed structure derived from pushover analysis. This curve is preliminarily transformed into the $V^*(=V_F/\Gamma)$-$d^*(d/\Gamma)$ curve of an equivalent SDOF system (Figure 5), being Γ the coefficient of participation of the first vibration mode,[41] and then idealised as bilinear, once yield and performance points are defined. Afterwards, the equivalent viscous damping due to hysteresis $\xi_{h,F}$ at the performance displacement can be calculated[42]

$$\xi_{h,F}(\%) = \kappa \cdot \left(63.7 \frac{(\mu_F - 1) \cdot (1 - r_F)}{\mu_F \cdot [1 + r_F \cdot (\mu_F - 1)]} \right) \tag{4}$$

as function of the following parameters (Figure 5b): ductility demand $\mu_F(=d^*_p/d^*_{y,F} = d_p/d_{y,F}$, being $d_{y,F}$ the yield displacement); stiffness hardening ratio (r_F); reduction factor (κ), depending on the degrading response of r.c. frame members.[37,38] An inherent elastic viscous damping of the framed structure (commonly, $\xi_{v,F} = 5\%$) can be also defined (Figure 5a).

Step 2. Properties of the SDOF system equivalent to the dissipative exoskeleton (DEX)

First and second columns with red boxes represent design and unknown parameters, respectively, of step 2 (Figure 4). Starting from the assumption that the stiffness (K_B) of the brace used to install the damper in the EX is large enough to eliminate the added stiffness of the FV damped brace (i.e., $K_{e,DB} \approx 0$, Figure 6a), the effective (secant) stiffness of the DEX is equal only to the EX part (Figure 6b)

$$K_{e,DEX} = K_{e,EX} \tag{5}$$

and its unknown value is assumed as the effective (secant) stiffness of the original frame multiplied by an initial value ($\alpha_K^{(0)}$) of the stiffness ratio:

$$K_{e,DEX}^{(0)} = \alpha_K^{(0)} \cdot K_{e,F} \tag{6}$$

Similarly, the effective mass of the equivalent DEX is obtained on the basis of an initial value ($\alpha_m^{(0)}$) of the mass ratio

$$m_{e,DEX}^{(0)} = \alpha_m^{(0)} \cdot m_{e,F} \tag{7}$$

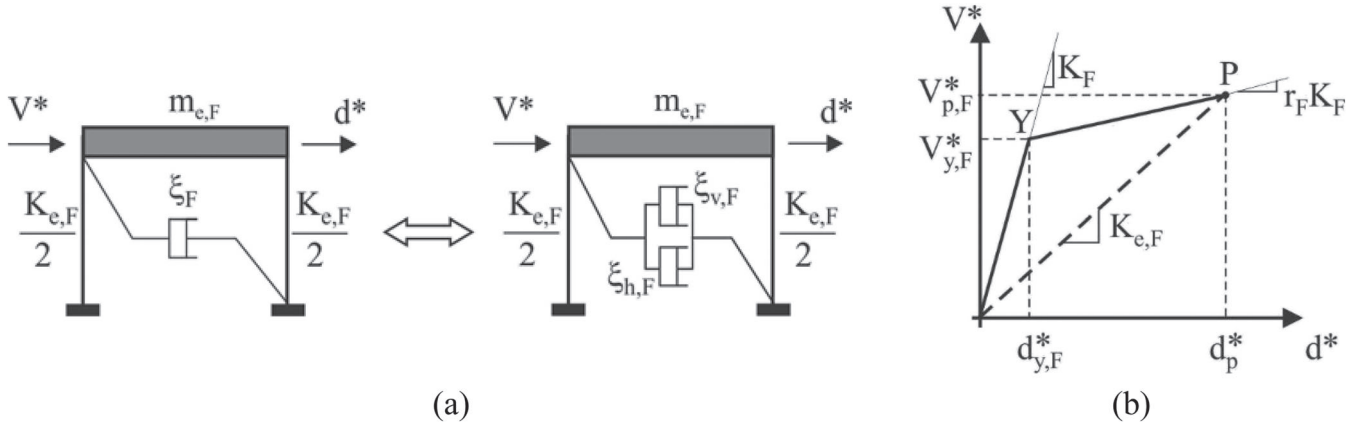

FIGURE 5 Equivalent SDOF system representing the original structure (a) and its response (b) idealised as bilinear

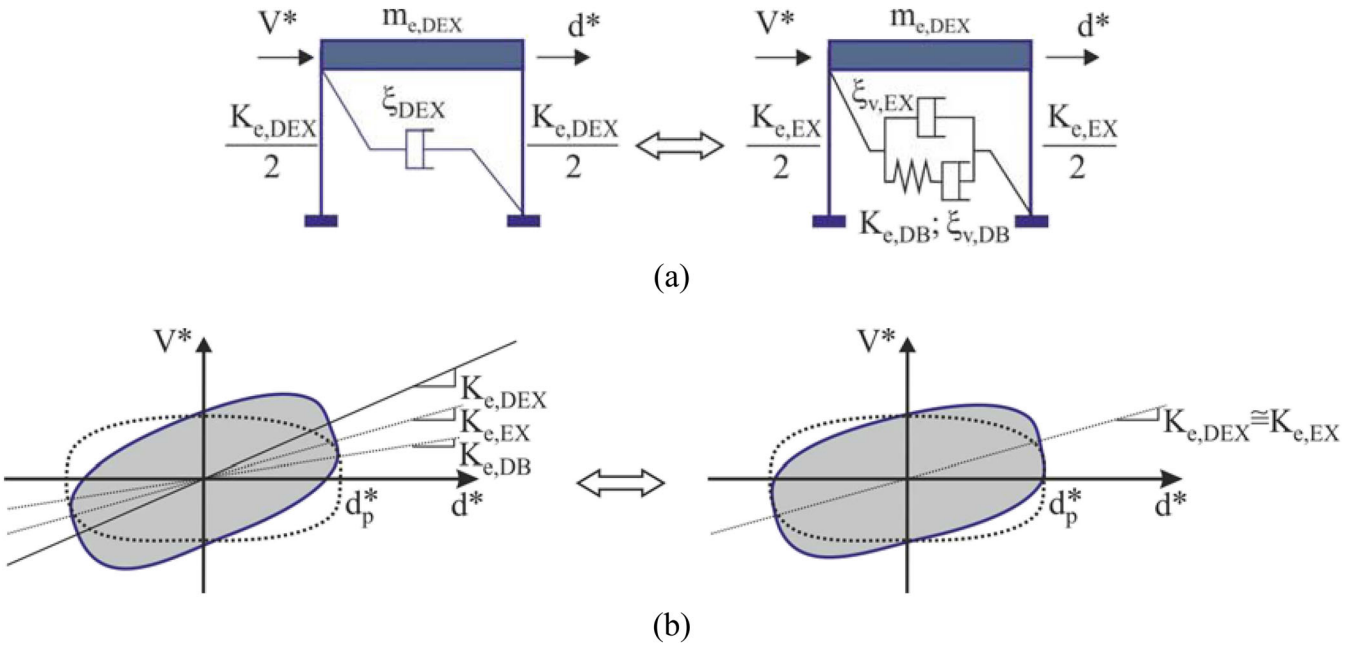

FIGURE 6 Equivalent SDOF system (a) representing the DEX and its non-elliptic hysteresis curve (b)

as function of the effective mass of the SDOF equivalent to the original frame (see Equation 2).

With regard to the nonlinear FVD, the force developed in the damper is function of the damping exponent ($\beta < 1$, with $\beta = 1$ corresponding to linear viscous property)

$$F_{VD} = C_{NL} \cdot sign(v) \cdot |v|^{\beta} = F_{VDB} \tag{8}$$

where C_{NL} is the nonlinear damping coefficient, v is the relative velocity between the end sections of the device and sign(v) is the sign function. Moreover, the equivalent viscous damping ratio for one cycle of harmonic vibration can be expressed on the basis of a non-elliptic hysteresis curve (Figure 6b).[1,43]

$$\xi_{v,DB}(\%) = \frac{\lambda \cdot C_{NL} \cdot \omega_{e,DEX}^{\beta} \cdot d_p^{\beta-1}}{2\pi \cdot K_{e,DEX}} \tag{9}$$

being

$$\lambda = 2^{2+\beta} \cdot \frac{\Gamma^2 \cdot \left(1 + \frac{\beta}{2}\right)}{\Gamma \cdot (2 + \beta)} \tag{10}$$

and Γ the gamma function. It is easy to verify that the equivalent viscous damping ratio corresponding to d_p can be computed in terms of an assigned maximum value ($\xi_{v,DB0}$) at the limit of elastic behaviour for the original frame:

$$\xi_{v,DB}(\%) = \xi_{v,DB0}(\%) \cdot (\mu_F)^{\beta-1} \tag{11}$$

For completeness, an inherent elastic damping of the EX (e.g., $\xi_{v,EX} = 2\%$ is generally used for steel structures) is also defined in Figure 6a.

Step 3. Properties of the SDOF system equivalent to the frame with dissipative exoskeleton (DEXF)

First and second columns with blue boxes shown in Figure 4 represent initial and intermediate (initially unknown) design parameters, respectively, while third column stores final unknown parameters. The equivalent viscous damping of the in-parallel system constituted of frame (F) and DEX is function of the stiffness ratio $\alpha_K^{(..)}$ ($=\alpha_K^{(0)}$ at the first iteration loop shown in step 2)

$$\xi_{DEXF}^{(..)}(\%) = \xi_{v,F}(\%) + \xi_{v,EX}(\%) + \frac{\xi_{h,F}(\%) + \xi_{v,DB}(\%)\cdot\alpha_K^{(..)}}{1+\alpha_K^{(..)}} \tag{12}$$

where $\xi_{h,F}$ and $\xi_{v,DB}$ are calculated in steps 1 (Equation 4) and 2 (Equation 11), respectively. Then, the effective period of DEXF ($T^{(..)}_{e,DEXF}$) is evaluated with reference to the curve of the overdamped displacement–acceleration design response spectra corresponding to $\xi^{(..)}_{DEXF}$ and the performance displacement d^*_p (Figure 7). Moreover, the acceleration design value ($a^{*}_{p}{}^{(..)}$) can be determined as y-coordinate by the same (red) curve.

Once the mass of the DEXF is calculated

$$m_{e,DEXF}^{(..)} = m_{e,F} + m_{e,DEX}^{(..)} = \left(1+\alpha_m^{(..)}\right)\cdot m_{e,F} \tag{13}$$

the effective stiffness can be obtained as follows:

$$K_{e,DEXF}^{(..)} = \frac{4\cdot\pi^2\cdot m_{e,DEXF}^{(..)}}{\left(T_{e,DEXF}^{(..)}\right)^2} \tag{14}$$

Finally, an updated value of the stiffness ratio is determined

$$\alpha_K^{(..)} = K_{e,DEX}^{(..)}/K_{e,F} \tag{15}$$

where

$$K_{e,DEX}^{(..)} = K_{e,DEXF}^{(..)} - K_{e,F}. \tag{16}$$

As a consequence, an iterative procedure internal to the current step is needed for the solution of Equations 12–16 until a final stiffness ratio value is attained.

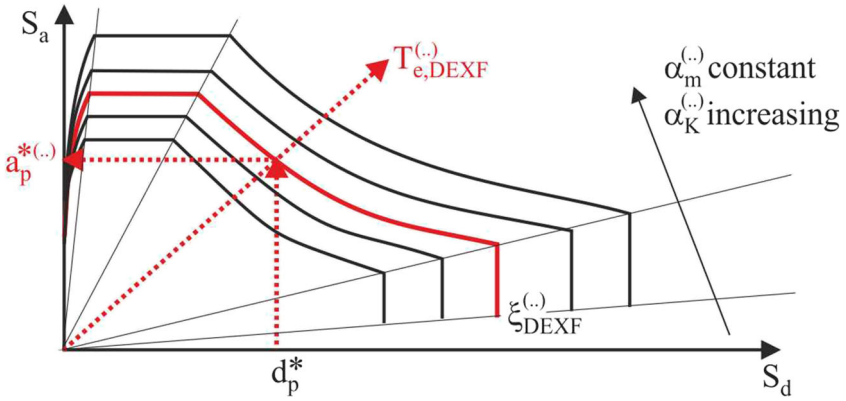

FIGURE 7 Displacement–acceleration overdamped (elastic) response spectra

Step 4. Properties of the dissipative exoskeleton (DEXF) for the MDOF system

Green boxes in Figure 4 correspond to step 4, on the assumption that stiffness of the CBF is proportional to that of the existing frame, to keep mode shapes and stress distribution of the DEXF practically unchanged, provided that regularity in elevation is satisfied.[44] Unlike traditional CBFs where brace buckling in compression and yielding in tension are the primary source of energy dissipation, often leading to poor dissipative behaviour to the detriment of heavy profiles for non-dissipative beams and columns connected to the bracing system,[45] an elastic-linear behaviour is assumed for all steel members by relying on the energy dissipation provided by the FVDs. The proportional stiffness criterion allows evaluation of the internal design forces of the steel EX considering the distribution of the lateral loads resulting from the first-mode shape (i.e., $\phi_i = \phi_{i,F} = \phi_{i,EX}$, i = 1,..,n) of the original structure that remains practically unchanged after the insertion of the EX (Figure 8)

$$F_{EX,i}^{(..)} = \frac{m_{i,F} \cdot \phi_i}{\sum_{i=1}^{n} (m_{i,F} \cdot \phi_i)} V_{d,EX}^{(..)} \tag{17}$$

where it is proved that the base-shear is equal to

$$V_{d,EX}^{(..)} = \frac{V_{d,DEXF}^{(..)} \alpha_K^{(..)}}{1 + \alpha_K^{(..)}} = \left(1 + \alpha_m^{(..)}\right) m_{e,F} \, a_p^{(..)} \frac{\alpha_K^{(..)}}{1 + \alpha_K^{(..)}} = V_{d,DEX}^{(..)}. \tag{18}$$

It is worth mentioning that base shear expressed by Equation 18 depends on the mass ratio $\alpha_m^{(..)}$, which is initially assumed equal to $\alpha_m^{(0)}$ in step 2. As a consequence, an external iterative procedure needs to be carried out on steps 3 and 4 for the solution of Equations 12–18, until a final mass ratio value is attained

$$\alpha_m^{(..)} = m_{e,DEX}^{(..)} / m_{e,F} = \sum_{i=1}^{n} \left(m_{i,DEX}^{(..)} \phi_i \right) / m_{e,F}, (\phi_n = 1). \tag{19}$$

Installation of the damping devices on additional chevron braces of the DEX (i.e., FVDB in Figure 8) appears a reasonable compromise among magnification of the damping effect, in comparison to the diagonal configuration, and its structural simplicity and compactness, with respect to the toggle-brace and scissor-jack systems.[46] Dimensions of the steel braces equal to those of the EX are selected, as a balance between opposing demands[47,48]: on the one hand,

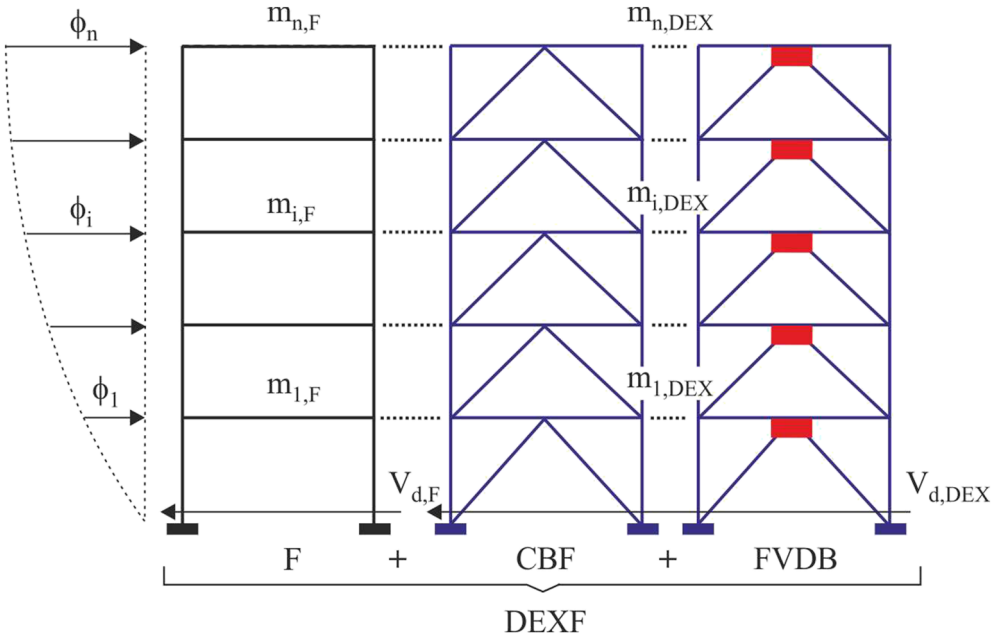

FIGURE 8 MDOF system representing the original frame (F) combined with DEX (CBF and FVDB)

reduction of stiffness can be related to functional and aesthetic requirements; on the other hand, increase of stiffness is required for activation of the energy dissipation and elimination of the added stiffness of the bracing system with FVDs.

Finally, the distribution of the damping coefficients for the nonlinear FVDs is assumed proportional to the design storey shear of DEX, through the following expression[30]

$$C_{NL,tot,j} = \frac{(2\pi)^{3-\beta}\cdot(d_p)^{1-\beta}\cdot\xi_{v,DB}}{(T_{1,DEXF})^{2-\beta}}\cdot\frac{S_j\cdot\sum_{i=1}^{n}(m_{i,DEXF}\cdot\phi_i^2)}{\lambda\cdot\sum_{i=1}^{n}\left[S_i f_i^{1+\beta}\cdot(\phi_i-\phi_{i-1})^{1+\beta}\right]},\ \mathrm{j}=1,..,\mathrm{n} \tag{20}$$

where f_i is the magnification factor of the dampers, depending on their configuration in each storey ($f_i = 1$ for chevron configuration of the FVDB) and $T_{1,DEXF}$ is the fundamental vibration period of DEXF. It is clear that at each storey the shear force is proportional to parameter[49]

$$S_j = \sum_{i=j}^{n}(m_{i,DEXF}\cdot\phi_i) \tag{21}$$

3 | THE ARCHETYPE

3.1 | Layout and design of the original frame

The archetype is a six-storey r.c. framed building located in L'Aquila, representative of the Italian residential housing stock constructed prior to the 2008–2018 code changes.[31] The building is regular in elevation (Figure 9b), while torsion is moderate so the building can be considered also as regular in plan although the staircase is asymmetrically placed along the X direction, and bays with different lengths are considered along the Y direction (Figure 9a).

Cross section of columns, with the orientation shown in Figure 9a, and deep beams, for perimeter frames and knee configuration of the staircase, are tapered along the building height but constant at each storey (Figure 9b); on the contrary, all internal beams are flat with a constant cross section at all storeys, but this is not the same for different bays (Figure 9a). Masonry infills with a double layer of hollow clay bricks only contribute to the dead load, with a weight of 3.5 kN/m^2 along the perimeter façades reduced as function of the percentage of apertures: that is, 0% for transversal façades; 40% for the first and five spans of longitudinal façades; 22% for the second and fourth spans of longitudinal façades. A simulated design of the test structure is carried out in line with the Italian codes IBC86,[50] for the seismic loads at the time corresponding to the medium-risk seismic zone and typical subsoil class. Provisions of the Italian code IBC92[51] are also satisfied, assuming the following gravity loads: dead loads of 4.8 kN/m^2, on the roof, and 6.3 kN/m^2,

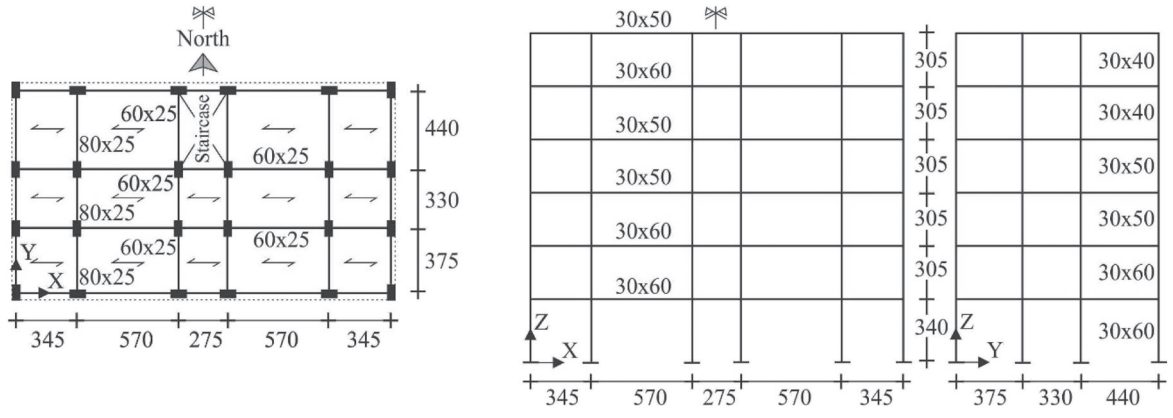

(a) Plan. (b) Elevation.

FIGURE 9 Layout of the archetype (unit in cm)

TABLE 1 Dynamic properties of the original structure (m_{tot} = 1566 t; $m_{tot,r} = 7.49 \times 10^{10}$ tm^2)

Mode	T (s)	$m_{e,X}$ (%m_{tot})	$m_{e,Y}$ (%m_{tot})	$m_{e,rZ}$ (%$m_{tot,r}$)
1	1.302	79	0	0
2	0.961	0	77	3
3	0.946	0	3	76
4	0.454	13	0	0
5	0.329	0	8	5

on the other floors; live loads of 2.2 kN/m^2, on the roof (snow), 2 kN/m^2, on the other floors, and 4 kN/m^2 for the staircase. Further details can be found in Ricci et al.[31]

Dynamic properties of the five main vibration modes are reported in Table 1: that is, vibration period (T); translational effective masses in the X ($m_{E,X}$) and Y ($m_{E,Y}$) directions and rotational effective mass around the Z direction ($m_{E,rZ}$), expressed as a percentage of the translation (m_{tot}) and rotational ($m_{tot,r}$) total masses, respectively. A torsionally stiff structure is found for both the X and Y directions, the ratio between the translational and torsional periods being greater than 1 as prescribed by the current Italian code IBC18.[49] Note that vibration periods correspond to the bare structure, where masonry infills are assumed as nonstructural elements only contributing with their weight. Moreover, reduced concrete elastic moduli are used for the beams ($E_{c,beam} = 0.5 \cdot E_c$) and columns ($E_{cm,columns} = 0.75 \cdot E_c$) in order to account for cracking of r.c. frame members.

Pushover curves of the original building are plotted in Figure 10, with reference to simplified nonlinear static analysis performed by the OpenSEES platform.[31,32] Since structural regularity criteria provided by IBC18 are satisfied,[52] invariant distributions of lateral loads monotonically increasing and proportional to the floor masses, with (i.e., 'modal') and without (i.e., 'uniform') considering the contribution of the first (elastic) vibration mode, are applied together with constant gravity loads. It should be noted that the top horizontal displacement is evaluated at the centre of mass along both in-plan directions, avoiding corner positions where negligible torsional effects are observed.

A lumped plasticity model is considered for r.c. frame members, with a trilinear moment-chord rotation backbone curve modified on the basis of the ultimate shear capacity in the event of brittle failure.[33,34] The shear behaviour of the exterior and interior beam-column joints is modelled by means of a scissor model, with rigid end offsets and double node, considering shear failure prior to or together with yielding of the longitudinal steel reinforcement of beams.[35,36] Mean compressive cylindrical strength of concrete and steel yield strength equal to 28 and 435 MPa are assumed, respectively, in the assessment of the capacity curves reported in Figure 10, representing roof drift ratio (i.e., d_{top}/H_{tot}, d_{top} and H_{tot} being the horizontal top displacement and total height) versus normalised base shear (i.e., V_{base}/W_{tot},W_{tot} being the total seismic weight). Note that pushover curves referring to the positive and negative loading directions are nearly identical, especially in the X direction (Figure 10a), due to the structural symmetry. Maximum strength is always achieved in the Y direction (Figure 10b), depending on the effects of the staircase and in-plan orientation of the cross sections of all interior columns and half of the exterior ones (Figure 9a), while maximum deformability is attained in the X direction (Figure 10a), where flat interior beams with reduced section are placed. Moreover, all modal and

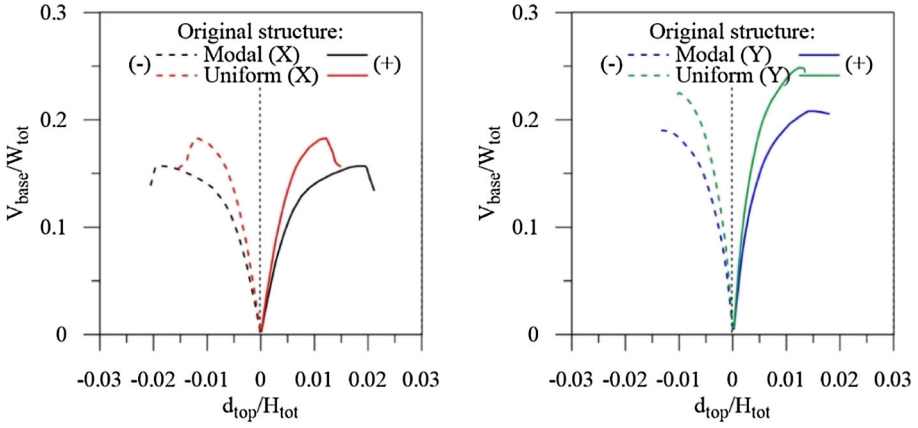

(a) X direction. (b) Y direction.

FIGURE 10 Comparison of pushover curves for modal and uniform lateral load patterns

uniform pushover analyses are terminated once the ultimate rotational capacity is achieved in columns at the first storey of the staircase. In the seismic retrofitting with DEX, attention will be focused on the modal capacity curves exhibiting a maximum V_{base}/W_{tot} ratio roughly between 0.15 (X direction) and 0.2 (Y direction) when the aforementioned failure mechanism is attained, contrary to 0.18 (X direction) and 0.25 (Y direction) corresponding to uniform capacity curves.

3.2 | Layout and design of the DEXs

Different retrofitting schemes involving a DEX are designed at the LS ultimate limit state provided by IBC18[52] for a residential building (functional class II, coefficient of use $C_U = 1.0$ and expected life of 50 years) located in L'Aquila (13.40° longitude and 42.35° latitude). Current high-risk seismic zone designation (peak ground acceleration on rock, $a_g = 0.261$ g) and moderately soft subsoil (class C, site amplification factor S = 1.33) are assumed. In particular, concentrically chevron braced frames (CBFs) and chevron braces with FVDs (FVDBs) are arranged in three configurations: (i) DEX.Pa (Figure 11), configured in adhesion (parallel) to all façades; (ii) DEX.Pe (Figure 12), as an enlargement of the entire building plan, creating additional (perpendicular) living space only along main fronts with apertures; (iii) DEX.Mi (Figure 13), where DEX.Pa and DEX.Pe are placed as an enlargement on the sides without apertures to satisfy both thermal and seismic requirements. Rigid connections are hypothesised between the new and old structures, although their sizing is not addressed in this study

The seismic demand for the design of the DEXs assumes as performance objective an elastic behaviour of the original structure (i.e., $d_p = d_y$ and $\xi_{h,F} = 0$). Specifically, performance displacement along the in-plan principal directions is evaluated from modal pushover curves as the value corresponding to the achievement of the first yielding condition in the r.c. frame members, also considering flexure–shear interaction failure mechanism (i.e., shear failure prior to or following flexural yielding). The amount of supplemental viscous damping required to limit maximum

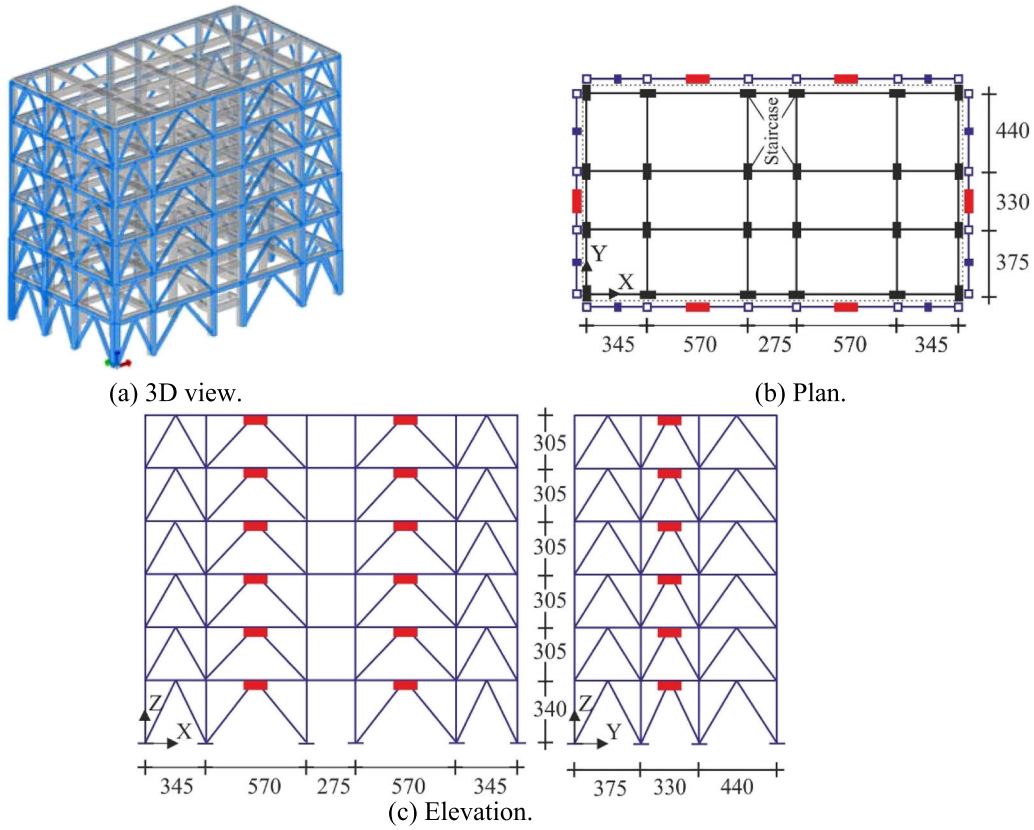

(a) 3D view. (b) Plan. (c) Elevation.

FIGURE 11 Dissipative exoskeleton parallel (DEX.Pa) to the original building (unit in cm): chevron brace and viscous damped chevron brace

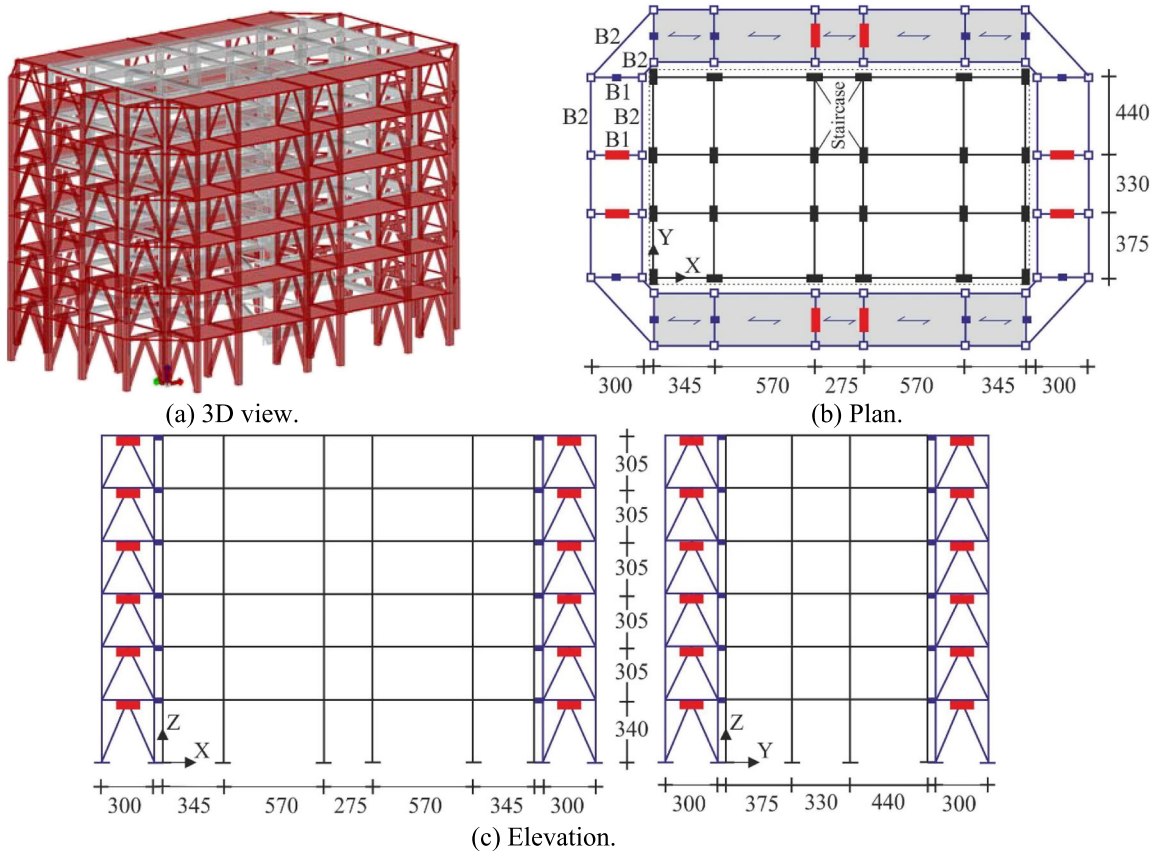

FIGURE 12 Dissipative exoskeleton perpendicular (DEX.Pe) to the original building (unit in cm): chevron brace and viscous damped chevron brace

displacement within this target value is assumed equal to $\xi_{v,DB0} = 20\%$, and elastic viscous damping of the EX is omitted. The stiffening contribution of the chevron braces arranged in series with the FVDBs is not considered while nonlinear viscous behaviour, with an exponent β equal to 0.7, is assumed for the FVDs. Structural redundancy required the insertion of two FVDBs on each side of the perimeter for DEX.Pe, while this condition is only met along the X direction for DEX.Pa and DEX.Mi. Moreover, interior bays of the EX are preferred as plan-wise location of the FVDBs in DEX.Pe and DEX.Mi, so as to reduce torsional deformability of the retrofitted structure through the insertion of CBFs in the exterior bays. The gravity loads considered for the composite deck with horizontal bracing of DEX.Pe, having a length of 3 m (see grey areas in Figure 12b), are represented by a dead load of 3.73 kN/m^2 and a live load of 2 kN/m^2. The design of DEXs is performed in accordance with the four-step double-iteration procedure presented below, and main parameters of the equivalent SDOF systems are reported in Tables 2 and 3 with reference to the X and Y directions, respectively. Note that an increase of mass (α_m) and stiffness (α_K) ratios corresponds to DEXF.Pe, while the same value is attained for DEXF.Pa and DEXF.Mi. As expected, all solutions have practically the same effective period ($T_{e,DEXF}$), with the highest value along the X direction, but maximum base shear ($V_{d,DEXF}$) always corresponds to DEX.Pe because of the additional mass of balconies along the X direction.

The tubular square cross sections selected for primary beams (i.e., typology B1), columns and chevron braces of the CBFs are assumed ductile, in line with class 1 of IBC18. These elements satisfy the ultimate limit states for strength and buckling under the horizontal seismic loads evaluated through Equations 17 and 18. Moreover, secondary (i.e., typology B2) beams with circular (DEX.Pe, Figure 12b) and square (DEX.Mi, Figure 13b) cross sections are also considered in order to obtain a spatial truss EX for which class 3 prevents local buckling until yield strength is reached in a compression fibre. The dimensions obtained for the member cross sections, assuming yield strength equal to 275 MPa, and damping coefficients of nonlinear FVDs are reported in Table 4 (DEX.Pa), Table 5 (DEX.Pe) and Table 6 (DEX.Mi). Comparison of the total amount of energy dissipation reveals that the highest values correspond to DEX.Pa and DEX.Pe for FVDs placed along the X and Y directions, respectively. It should be noted that FVDs are inserted on chevron braces with the same dimensions as those of the CBFs.

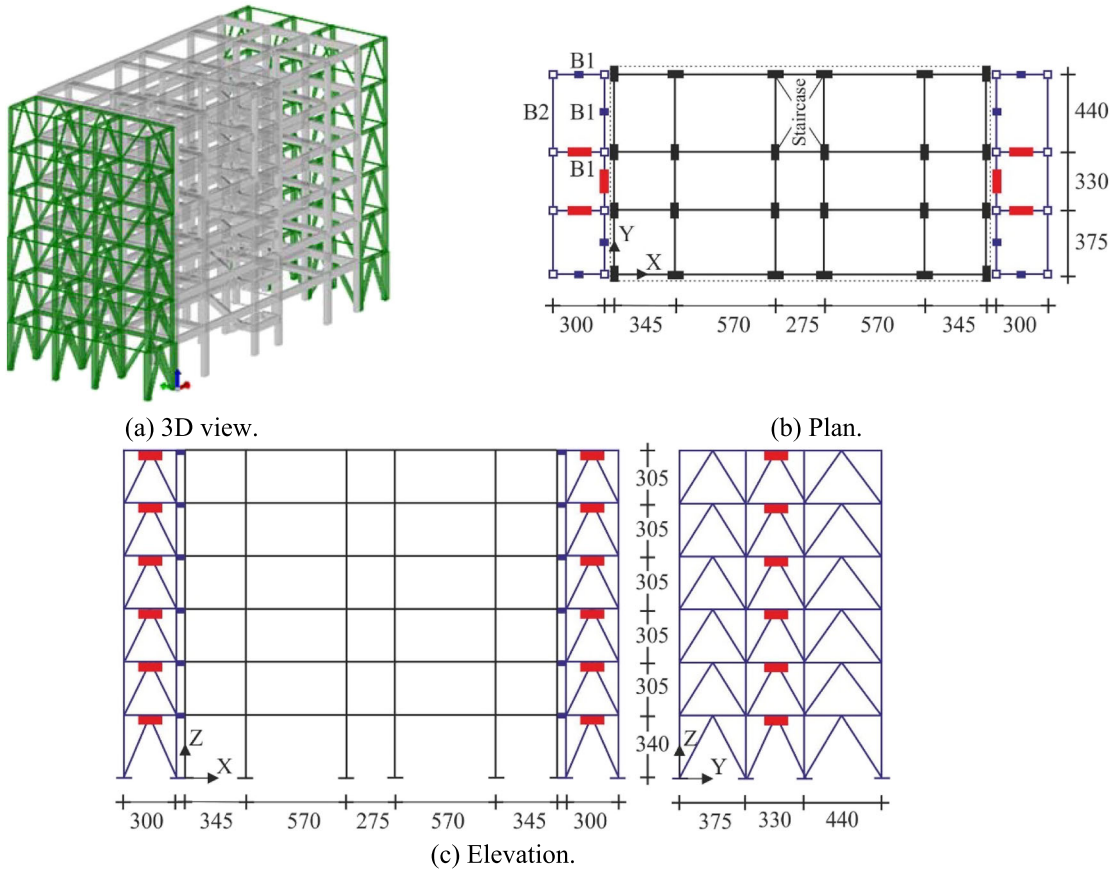

FIGURE 13 Dissipative exoskeleton with a mixed configuration (DEX.Mi) around the original building (unit in cm): chevron brace and viscous damped chevron brace

TABLE 2 Main properties of the SDOF system equivalent to DEXF along the X direction (units in cm, kN, t and s)

Structure	d^*_p	a^*_p	μ_F	$K_{e,F}$	$m_{e,F}$	$\xi_{h,F}$	α_m	α_K	β	$\xi_{v,DB0}$	$\xi_{v,DB}$	ξ_{DEXF}	$T_{e,DEXF}$	$V_{d,DEXF}$
DEXF.Pa	2.91	486	1	213	931	0	0.034	6.55	0.7	20	20	22.4	0.487	4678
DEXF.Pe	2.91	481	1	213	931	0	0.289	8.33	0.7	20	20	22.9	0.489	5778
DEXF.Mi	2.91	486	1	213	931	0	0.042	6.60	0.7	20	20	22.4	0.487	4709

TABLE 3 Main properties of the SDOF system equivalent to DEXF along the Y direction (units in cm, kN, t and s)

Structure	d^*_p	a^*_p	μ_F	$K_{e,F}$	$m_{e,F}$	$\xi_{h,F}$	α_m	α_K	β	$\xi_{v,DB0}$	$\xi_{v,DB}$	ξ_{DEXF}	$T_{e,DEXF}$	$V_{d,DEXF}$
DEXF.Pa	1.48	486	1	414	923	0	0.034	6.55	0.7	20	20	22.4	0.347	4638
DEXF.Pe	1.48	481	1	414	923	0	0.289	8.32	0.7	20	20	22.9	0.349	5728
DEXF.Mi	1.48	486	1	414	923	0	0.042	6.60	0.7	20	20	22.4	0.347	4668

4 | NUMERICAL RESULTS

The nonlinear seismic response of the structure before (i.e., original, F) and after (i.e., retrofitted, DEX.Pa, DEX.Pe and DEX.Mi) the insertion of the DEX is evaluated by the finite element code OpenSEES.[32] Hysteretic models that incorporate strength and stiffness degradation are considered for r.c. frame members,[33] ModIMKPeakOriented material, and joints,[35] Pinching4 uniaxial material, including ductile (flexural) and brittle (shear) failure modes. Nonlinear FVDs are modelled as twoNodeLink elements, assuming nonlinear dashpot and linear spring acting in series without considering

TABLE 4 Member cross sections (unit in mm) and damping coefficient of FVDs (units in kN, s and m) for DEX.Pa

			Chevron braces		$C_{NL,tot}$ (FVDs)	
Storey	Beams	Columns	X direction	Y direction	X direction	Y direction
1	250 × 8	350 × 16	220 × 16	220 × 16	9999	9118
2	250 × 8	300 × 12.5	180 × 12.5	180 × 12.5	9657	8818
3	200 × 8	260 × 10	180 × 10	180 × 10	8839	8092
4	200 × 8	220 × 8	180 × 8	160 × 10	7438	6830
5	200 × 8	220 × 8	180 × 6.3	150 × 8	5388	4976
6	200 × 8	220 × 8	160 × 6.3	150 × 6.3	2702	2513

TABLE 5 Member cross sections (unit in mm) and damping coefficient of FVDs (units in kN, s and m) for DEX.Pe

	Beams			Chevron braces		$C_{NL,tot}$ (FVDs)	
Storey	B1	B2	Columns	X direction	Y direction	X direction	Y direction
1	350 × 10	88.9 × 5	400 × 20	350 × 16	300 × 12.5	8467	11,545
2	300 × 10	88.9 × 5	350 × 16	260 × 12.5	260 × 8	8209	11,199
3	300 × 10	88.9 × 5	300 × 10	220 × 12	250 × 6.3	7619	10,322
4	200 × 8	88.9 × 5	300 × 10	180 × 12.5	220 × 6.3	6533	8750
5	200 × 8	88.9 × 5	220 × 8	150 × 12.5	180 × 6	4854	6421
6	200 × 8	88.9 × 5	220 × 8	140 × 12	140 × 6.3	2496	3299

TABLE 6 Member cross sections (unit in mm) and damping coefficient of FVDs (units in kN, s and m) for DEX.Mi

	Beams			Chevron braces		$C_{NL,tot}$ (FVDs)	
Storey	B1	B2	Columns	X direction	Y direction	X direction	Y direction
1	300 × 10	50 × 5	400 × 16	260 × 16	250 × 16	8424	10,753
2	250 × 10	50 × 5	300 × 16	220 × 12	180 × 12.5	8178	10,370
3	250 × 10	50 × 5	260 × 10	200 × 10	180 × 10	7560	9442
4	200 × 8	50 × 5	220 × 8	150 × 12	180 × 8	6443	7894
5	200 × 8	50 × 5	220 × 8	120 × 12.5	150 × 8	4738	5675
6	200 × 8	50 × 5	220 × 8	120 × 12	150 × 6.3	2407	2821

the combined flexibility of the supporting brace and FVD. An elastic-linear behaviour, equal for tension and compression, is considered for all truss members of the concentrically steel braced frames. The EX is connected to the r.c. framed building at each floor level by means of shear and/or axial rigid steel links. Inherent damping $\xi_{v,F} = 5\%$ for the r.c. framed structure is modelled using mass and tangent stiffness proportional Rayleigh approach,[31] while the contribution of steel EX is not considered ($\xi_{v,EX} = 0\%$).

Seismic input selection for the bidirectional nonlinear dynamic analyses considers earthquakes taken from the Italian accelerometric archive[53] and NGAwest2 database,[54] the latter when records reflecting the IBC18 provisions at the site in question were not available, and scaled to match the LS design response spectrum.[55] The following results are obtained as the mean of the maximum values obtained for each pair of accelerograms. Modal analysis of the DEXF structures is carried out at the first step of the study. Dynamic properties of the four main vibration modes for DEXF. Pa, DEXF.Pe and DEXF.Mi, two for each principal in-plan direction, are reported in Table 7 together with the total mass of the retrofitted building (m_{tot}): that is, vibration periods (T_{iX} and T_{iY}, i = 1,2) and translational effective mass (m_{iX} and m_{iY}, i = 1,2), expressed as a percentage of m_{tot}. The similarity of the effective masses of the first two translational modes (i.e., m_{1X} and m_{1Y}) to those obtained for the original structure is confirmed with a slight albeit

TABLE 7 Dynamic properties of the retrofitted test structures (units in t and s)

Structure	m_{tot}	T_{1X}	m_{1X} (%m_{tot})	T_{1Y}	m_{1Y} (%m_{tot})	T_{2X}	m_{2X} (%m_{tot})	T_{2Y}	m_{2Y} (%m_{tot})
DEXF.Pa	1631	0.551	73	0.506	72	0.192	18	0.179	18
DEXF.Pe	2051	0.686	68	0.479	70	0.268	23	0.167	20
DEXF.Mi	1649	0.599	70	0.455	74	0.208	20	0.163	16

unavoidable difference, due to the use of commercial profiles for steel members instead of the effective area resulting from the proportional stiffness criterion. Two vibration modes are needed to activate summed modal masses greater than 85%m_{tot} along both directions in plan. Torsional deformability is avoided in all structural schemes, with logical arrangement of FVDs in the internal frames that is found necessary for DEX.Pe, in particular with regard to the Y direction (Figure 12b).

4.1 | Preliminarily check of the design assumptions for the DEXs

First, mean values of the maximum base shear are reported in Figure 14 for the original (F) and retrofitted (DEX (F) and (DEX)F referring to parallel (Pa), perpendicular (Pe) and mixed (Mi) steel DEX and r.c. frame, respectively) structures, which are labelled with letter A when resulting from nonlinear time-history analysis. As a comparison, design values (letter D) of the base shear obtained for DEXs (see Equation 18) are also reported with reference to DEXF.Pa (Figure 14a,d), DEXF.Pe (Figure 14b,e) and DEX.Mi (Figure 14c,f). The proportion between the base shear corresponding to DEX(F)_A and (DEX)F_A structural parts highlights a good fit with the design value of the stiffness ratio α_K (see Tables 2 and 3), thus confirming the reliability of the design procedure of DEXs. This is further demonstrated by the ratio between design (D) and analysis (A) base shear for DEX, whose value falls approximately into the

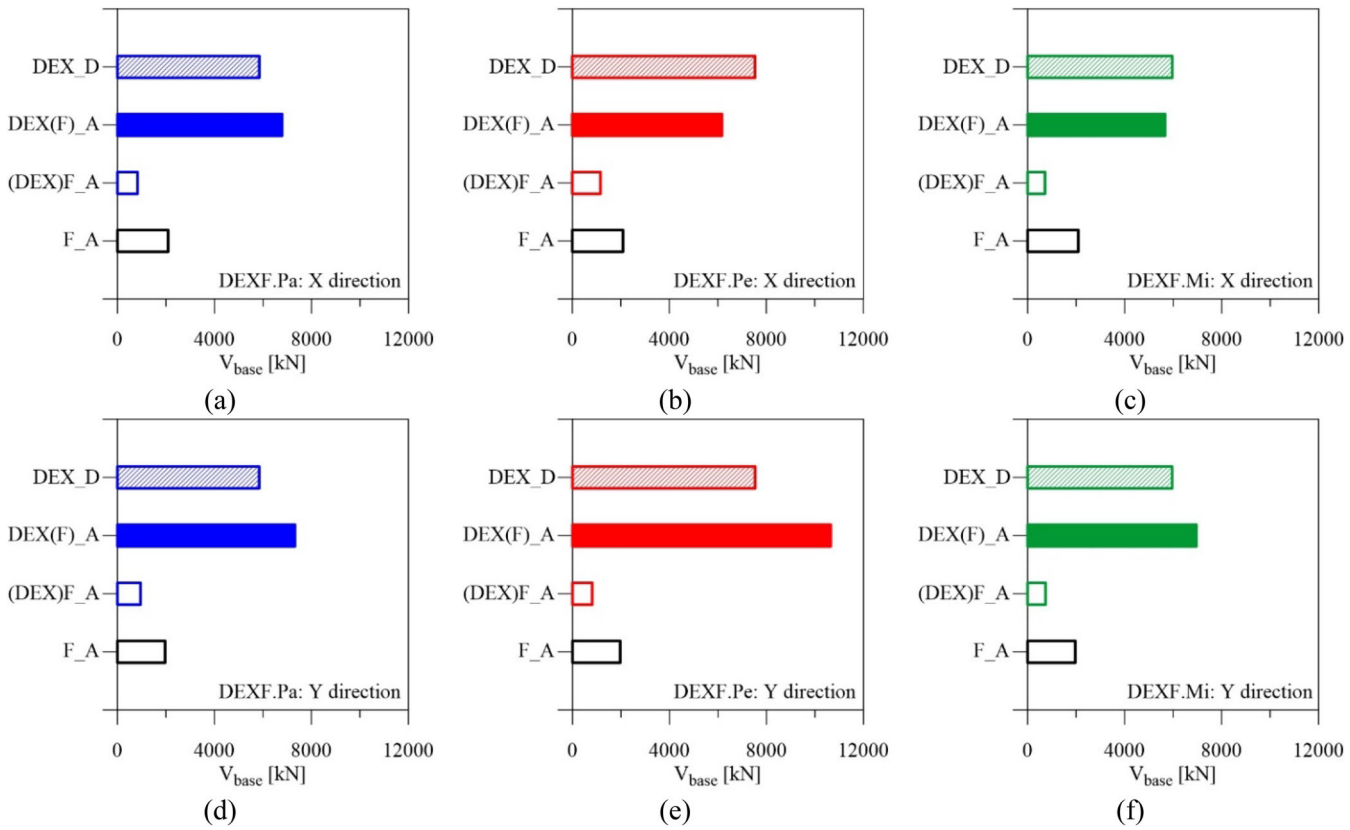

FIGURE 14 Seismic demand in terms of base shear for the original (F) and retrofitted (DEXF) structures

range of −10% to +30%, which represent the lower and upper bound tolerances provided by IBC18 when recorded ground motions are scaled to a certain level of seismic intensity. Evidence of the effectiveness of the proposed retrofitting strategies also results from base shear related to (DEX)F_A, whose value is between one half (Figure 14e) and one third (Figure 14c) of that given to the corresponding F_A.

Once the shear of DEXs resulting from nonlinear seismic analysis is determined, local behaviour of the CBFs is examined to assess the most critical ultimate limit states of the main steel truss members. To this end, in Figures 15–17, the mean of the maximum values attained by the safety factors controlling yielding and buckling are plotted along the EX height and for both in-plan directions (i.e., X_A and Y_A). Specifically, tensile and compressive axial forces induced by the seismic loads in the chevron braces (Figures 15a,d, 16a,d and 17a,d), columns (Figures 15b,e, 16b,e and 17b,e) and beams (Figures 15c,f, 16c,f and 17c,f) are divided by the corresponding tension (yielding) and compression (buckling) resisting forces calculated in line with IBC18. It should be noted that the same value of the safety factory is plotted for columns of DEX.Mi along X (Figure 17b) and Y (Figure 17e) directions, differently from DEX.Pa (Figure 15b,e) and DEX.Pe (Figure 16b,e) where distinction is possible between columns corresponding to each of the two couple of façades. Curves representing analogous design values (i.e., X_D and Y_D) are also reported with dotted lines, with reference to DEX.Pa (Figure 15), DEX.Pe (Figure 16) and DEX.Mi (Figure 17). As can be observed, the minimum (absolute value) and maximum axial forces (solid lines) deriving from nonlinear seismic analysis are less than the yielding and buckling IBC18 thresholds (i.e., the $|N_{min}|/N_{yielding}$ and $N_{max}/N_{buckling}$ ratios are less than 1) for all the truss members. This fully supports the design assumption made with reference to the elastic behaviour of the EX under seismic loads, as confirmed by X_D and Y_D curves (black dotted lines). Moreover, the ratio between the maximum axial load of chevron braces resulting from the design and analysis follows very closely the analogous ratio calculated with reference to the base shear (see Figure 14). As an example, DEX.Pe is characterised by greater Y_A values than Y_D ones, for both $|N_{min}|/N_{yielding}$ (Figure 16a) and $N_{max}/N_{buckling}$ (Figure 16d), while the opposite happens

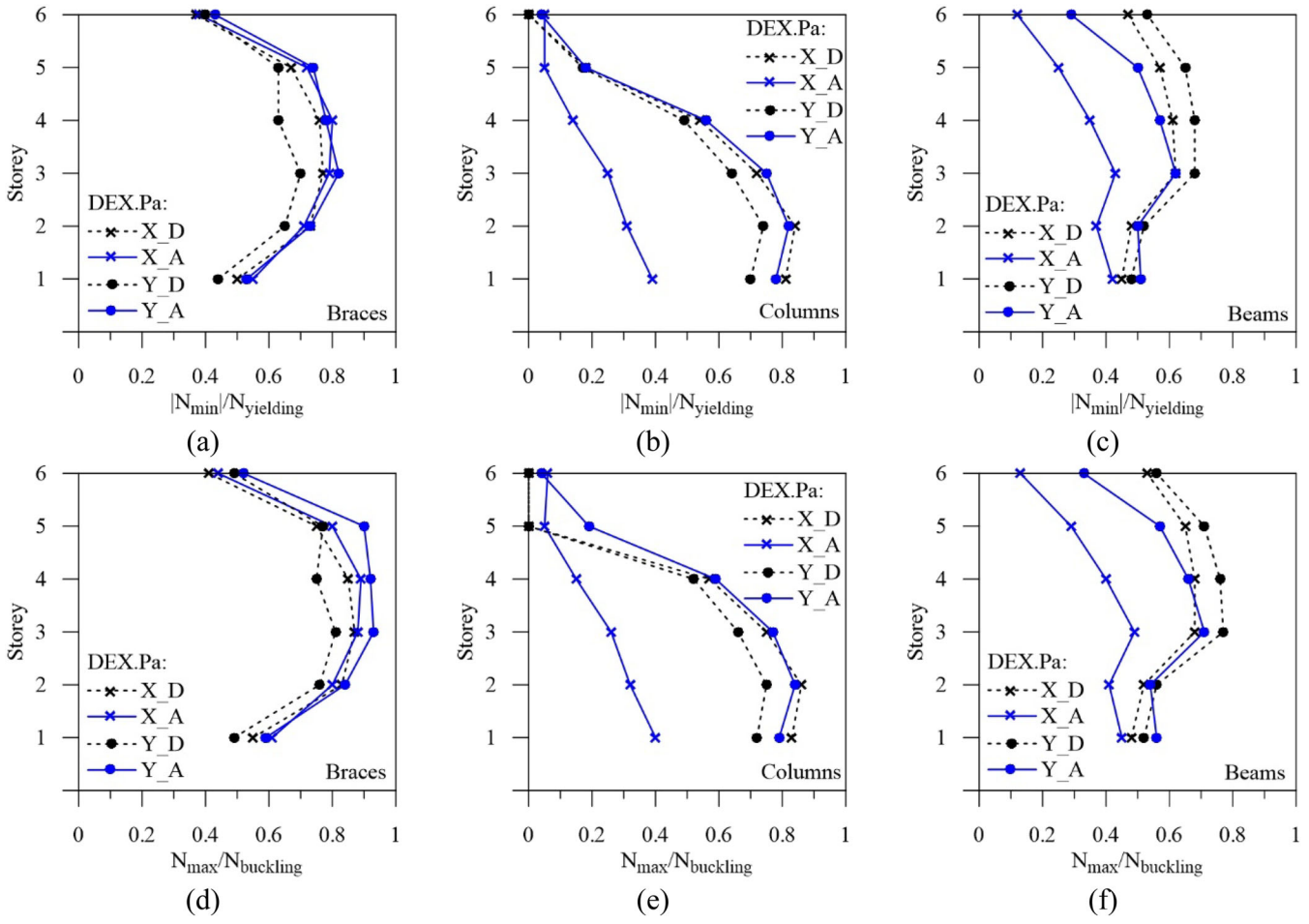

FIGURE 15 Safety factors against yielding (a–c) and buckling (d–f) for truss members of DEX.Pa

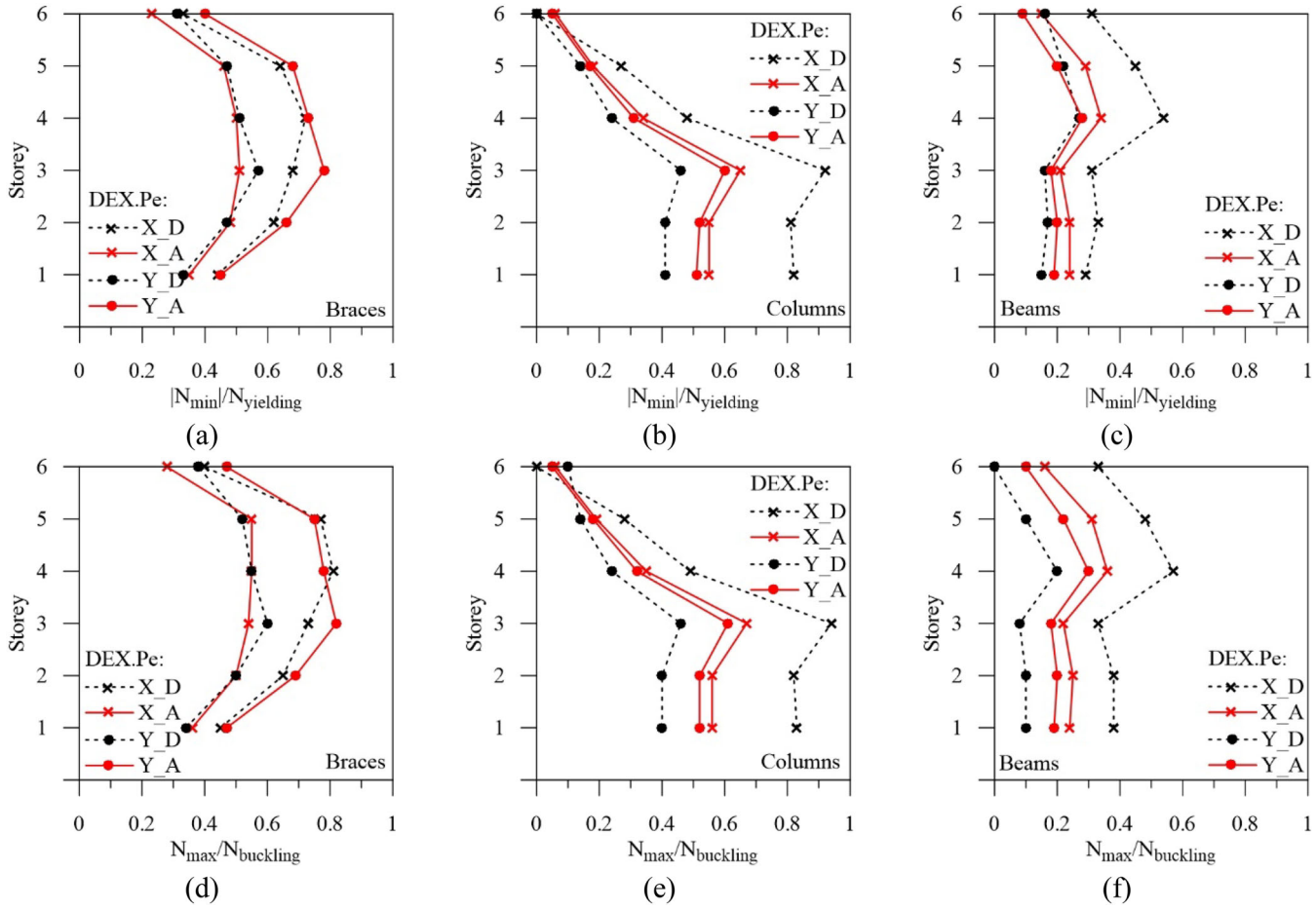

FIGURE 16 Safety factors against yielding (a–c) and buckling (d–f) for truss members of DEX.Pe

with X_A and X_D, confirming the trend already observed for the base shear (Figure 14b,e). Contrary to what may be expected, differences are observed between the vertical distribution of axial loads in the truss members of DEX.Pa and DEX.Mi and DEX.Pe and DEX.Mi, along Y and X, respectively. This is explained by the fact that the three-dimensional reticular structure of DEX.Mi behaves differently from the bidimensional scheme of DEX.Pa, while DEX.Pe is characterised by additional masses of the balconies of the main façades not included in DEX.Mi. One interesting point regards the axial load in the columns, whose intensity is greater for DEX.Pa (Figure 15b,e) than DEX.Pe (Figure 16b,e) and DEX.Mi (Figure 17b,e) due to overturning moments induced by seismic loads. As expected, tensile axial loads are transmitted to the foundation system of all DEXs, thus requiring the insertion of piles, with DEX.Pe being the most attractive solution because of additional gravity loads in comparison to the other configurations. Note that an increase of width of the chevron-braced bays induces high lateral stiffness of DEX and decreases axial load in the columns, while it makes it more difficult to control the buckling of chevron braces and increases the axial load transmitted to the beams.

4.2 | Final check of strength and weaknesses of the DEXs

Afterwards, mean values of the storey drift ratio, defined as drift along the in-plan X (Δ_X) and Y (Δ_Y) directions normalised by the storey height (h), are shown in Figure 18. The original structure (F) exhibits an irregular distribution law of the drift ratio, with higher deformability in the X (Figure 18a) rather than in the Y (Figure 18d) direction. The insertion of DEXs generally ensures a reduction of at least half of the drift demand, the values being in the range of light ($0.2\% < \Delta_{max}/h < 0.4\%$) and moderate ($0.4\% < \Delta_{max}/h < 1\%$) repairable damage at lower and intermediate levels, respectively.[56] The only exception is the top floor where an increase in drift demand referring to Y is observed for DEX.Pa and DEX.Pe (Figure 18d), though highlighting values less than 0.5%. This result may well depend on the reduced

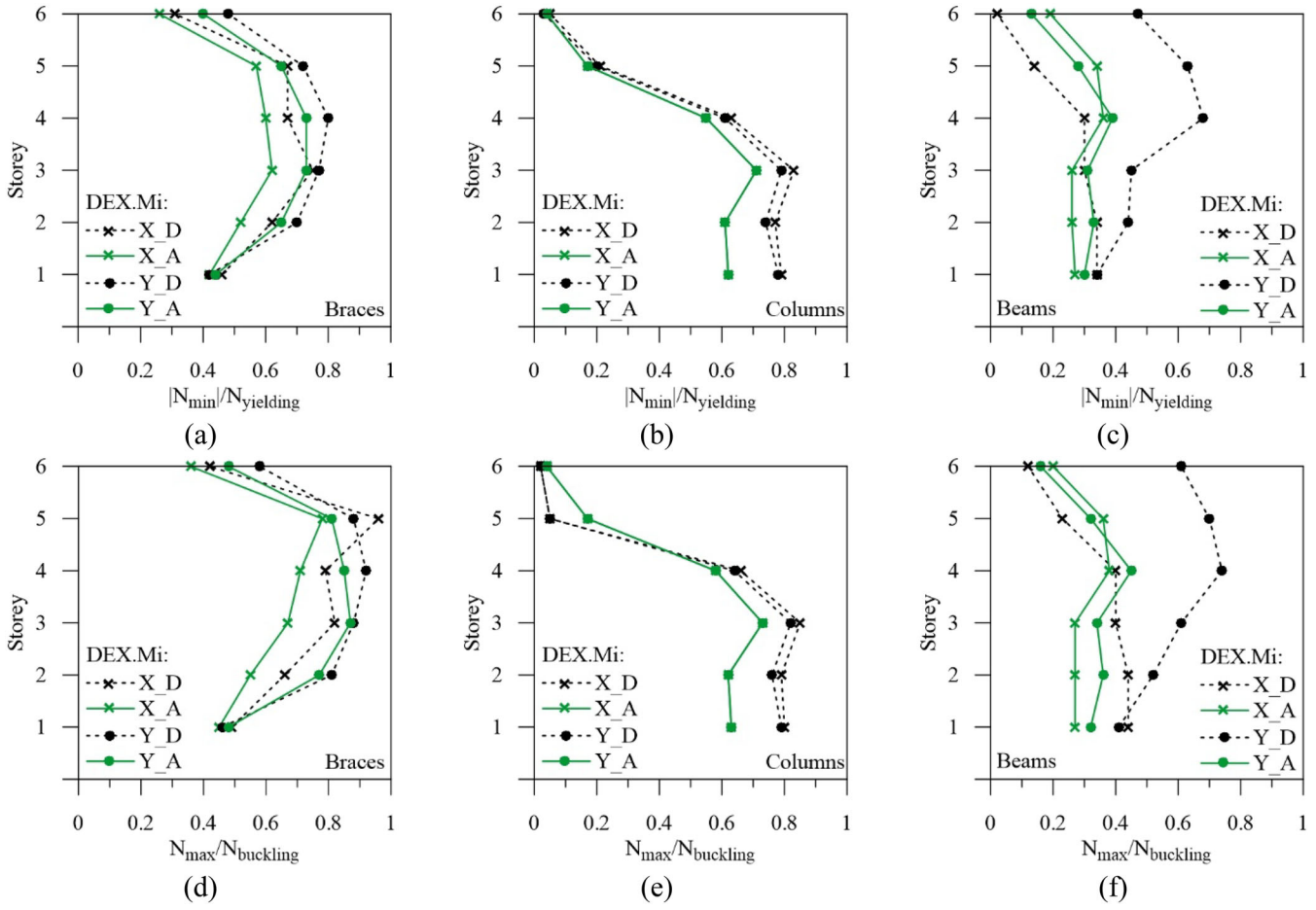

FIGURE 17 Safety factors against yielding (a–c) and buckling (d–f) for truss members of DEX.Mi

energy dissipation of FVDs on the top floor compared to those below, because reduced interstorey velocity. Among the three viable retrofitting schemes, DEXF.Pa and DEX.Mi turn out to be the best choice parallel to X (Figure 18a) and Y (Figure 18d), respectively, which is justified by the combination of low stiffness and mass ratios of the EX and high damping coefficients of the FVDs. Graphs of horizontal displacement at the floor levels (Figure 18b,e) confirm the effectiveness of all configurations of the DEX, with DEX.Mi representing the solution that is closest to the performance displacement at the roof level corresponding to full operational serviceability (FO) limit state provided by IBC18 (i.e., $d_{top,FO} = 6.2$ cm). The acceleration profiles over the elevation of the building, normalised by gravity acceleration g, are displayed in Figure 18c,f. Amplification of acceleration is found in all DEXF systems compared to the original frame, with values increasing towards the upper levels where this may represent a potential risk for the protection of acceleration-sensitive nonstructural components. Moreover, a clear worsening is observed in the Y direction (Figure 18f), where DEX.Pe is the worst solution inducing a threefold increase in top floor acceleration.

With a view to analysing how different configurations of the DEX (i.e., DEX.Pa, DEX.Pe and DEX.Mi) have an impact on the effectiveness of FVDs, the mean of the maximum values of the total damping force at different storeys is shown in Figure 19. As confirmed experimentally,[30] the efficiency of the FVDs in the top storey is reduced by at least half of that at the intermediate levels where maximum values are attained, thereby highlighting that a distribution of damping constants proportional to the storey shear represents an efficient design criterion. The highest energy dissipation corresponds to DEX.Pa and DEX.Pe in the X (Figure 19a) and Y (Figure 19e) directions, respectively, but this does not correspond to significant advantages for the DEX.Pe characterised by the additional mass of balconies. It should be noted that total damping force is only divided between two FVDs for DEX.Pa (Figures 11b and 19d) and DEX.Mi (Figures 13b and 19f) along the Y direction, thus reducing structural redundancy, contrary to DEX.Pe which instead provides four FVDs at each level (Figures 12b and 19e), while all solutions ensure the same number of FVDs in the X direction.

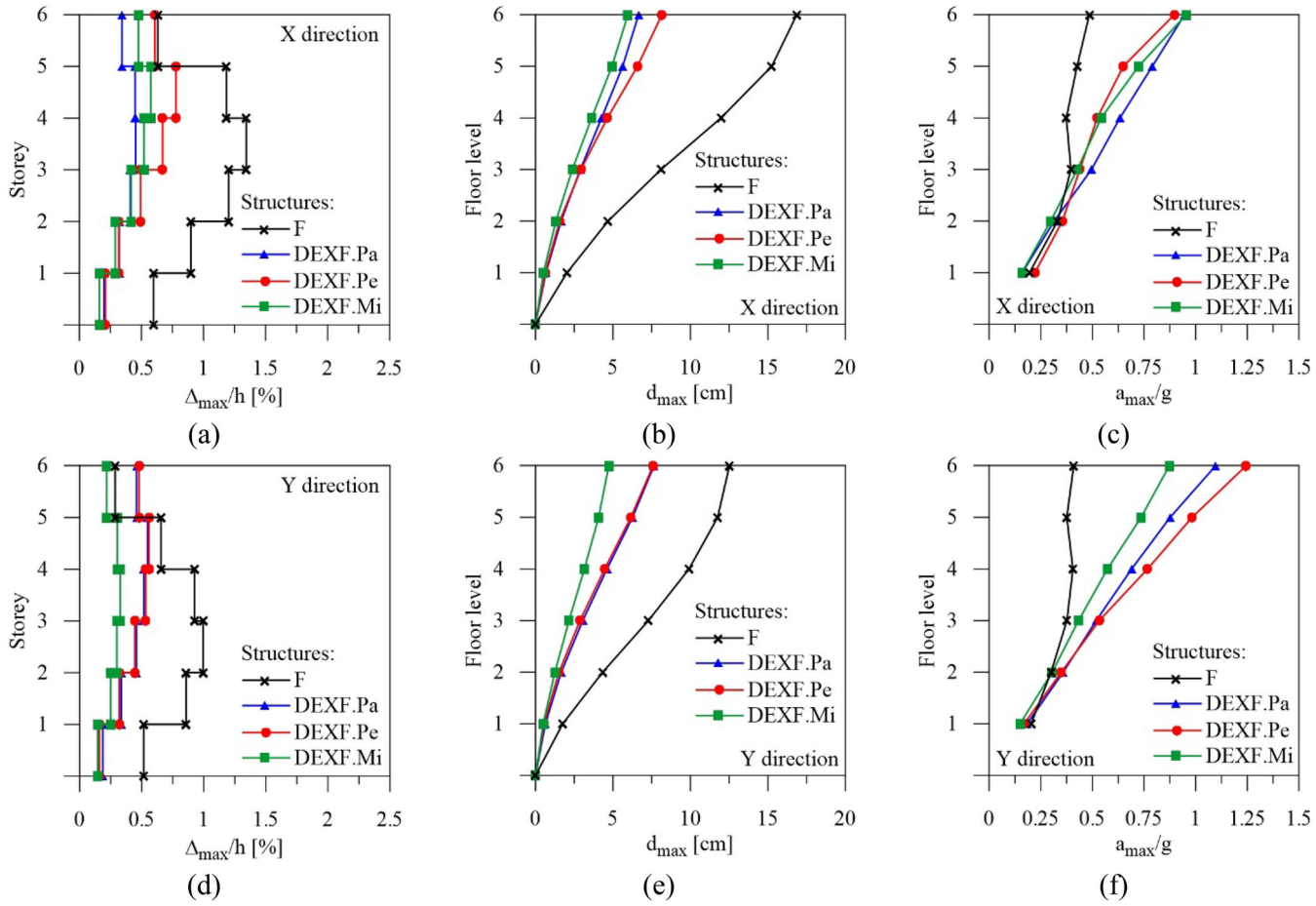

FIGURE 18 Global response parameters of the original (F) and retrofitted (DEXF) structures over the elevation

Next, time evolution of the top displacement (d_{top}) for the centre of mass of the original (F) and retrofitted (DEXF.Pa, DEXF.Pe and DEXF.Mi) buildings is shown in Figure 20a,b, with reference to the two horizontal components of the earthquake matching the LS design spectrum more closely than the other selected earthquakes. Curves corresponding to the principal in-plan directions are plotted separately in Figure 20a (X) and 20b (Y). Target value of the retrofit displacement (d_p), corresponding to elastic behaviour of the r.c. framed structure, is also represented by dotted lines. This threshold is exceeded many times by the building in its original condition, confirming that inelastic behaviour characterises the dynamic response. On the other hand, it is practically observed by all retrofitting solutions when Y direction is considered, while only DEXF.Pa and DEXF.Mi are consistent with this value along X direction. Finally, time history of d_{top} for the couples of corner joints of DEXF.Pe is plotted in Figure 20c (X) and 20d (Y) to investigate the effects of the in-plan configuration of FVDs on its torsional response. Specifically, two configurations of FVDs are compared: that is, central position in both horizontal directions (DEXF.Pe_A, Figure 12); central (X) and intermediate (Y) positions (DEXF.Pe_Bi, i = 1,2). As can be observed, torsional effects due to the eccentric position of the r.c. staircases are avoided in the case of central configuration of FVDs (A), thanks to the external arrangement of chevron braces of the CBFs. However, torsional deformability and significant difference of corner displacements are obtained when the intermediate (B) solution is considered, highlighting the fact that the correct choice of in-plan disposition of CBFs and FVDs is crucial. Further results, omitted for the sake of brevity, have underscored the fact that 'strong-beam weak-column' mechanism and high shear demand in the beam-column joint panels are obtained at lower and intermediate levels of the original r.c. building, respectively. For all the examined cases, the insertion of the DEXs is an effective means of upgrading capacity, ensuring a notable reduction of the seismic demand at the critical end sections of r.c. beams and columns and in the joints and avoiding both ductile and brittle failure modes.

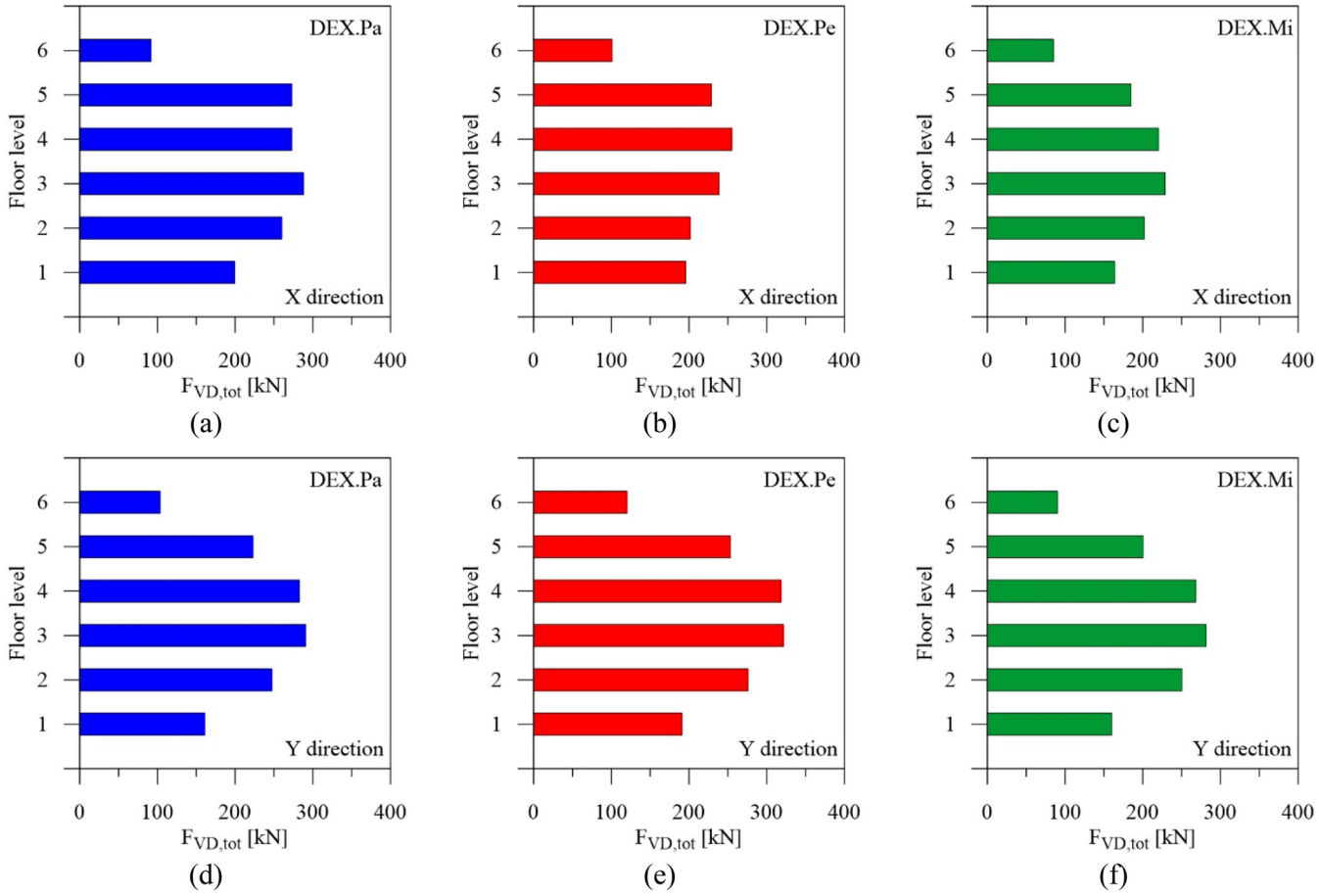

FIGURE 19 Distribution of the total damping force of FVDs over the elevation of the DEXs

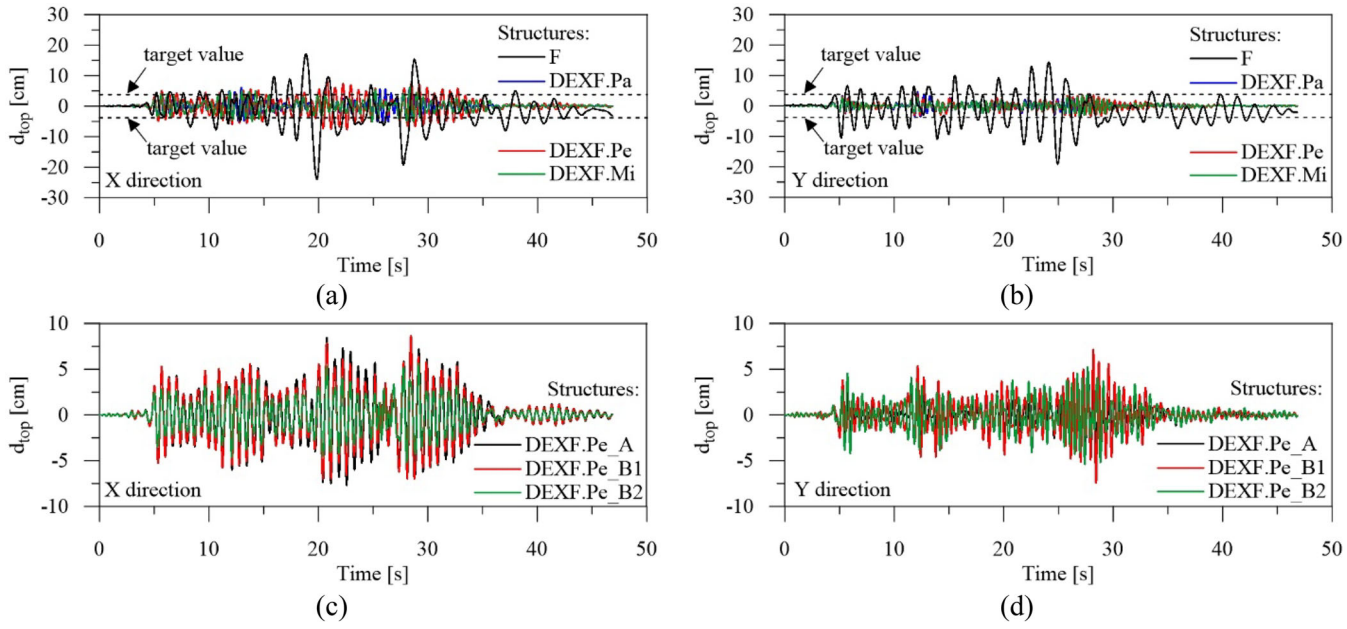

FIGURE 20 Time histories of top displacement for the original (F) and retrofitted (DEXF) structures

5 | CONCLUSIONS

This work intends to examine seismic retrofitting of r.c. buildings by attaching DEX made with concentric steel braced frames and FVDs. To this end, a practical procedure for the seismic design is proposed and developed, in such a way as to make a distinction between the steel EX and the dissipative bracing system. A six-storey r.c. framed structure located in L'Aquila is assumed as an archetype of the residential housing stock built in Italy during the 1990s, designed for medium-risk seismic zone. Three configurations of the DEX along the perimeter are chosen for retrofitting the original building, assuming elastic behaviour as performance objective in a high risk-seismic zone: that is, DEX.Pa, representing an envelope parallel to all façades that minimises the external dimension in the presence of urban planning restrictions; DEX.Pe, perpendicular to all façades and enjoying an outdoor space along main fronts with apertures; DEX.Mi, suggested as a compromise solution in which DEX.Pa and DEX.Pe are only placed on the sides without apertures to reduce the impact on the existing building and satisfy thermal requirements. By carrying out nonlinear seismic, the following conclusions can be drawn.

The proportion between base shear demands corresponding to DEX(F) and (DEX)F structural parts matches well with the design value of the stiffness ratio, thus confirming the reliability of the proposed design procedure. Further, positive evidence is found when checking safety factors of the main steel truss members against yielding and buckling along the EX height and for both in-plan directions. Although the external positions are the same, differences are observed between the vertical distribution of axial loads in the truss members of DEX.Pa and DEX.Mi, along Y, and DEX.Pe and DEX.Mi, along X. This is explained by the fact that the three-dimensional reticular structure of DEX.Mi behaves differently from the bidimensional scheme of DEX.Pa, while DEX.Pe is characterised by additional masses of the balconies not included in DEX.Mi. An interesting point regards the axial load in the columns, whose intensity is greater for DEX.Pa than DEX.Pe and DEX.Mi due to overturning moments induced by seismic loads. Moreover, tensile axial loads are transmitted to the foundation system of all DEXs, thus requiring the insertion of piles, DEX.Pe resulting the most attractive solution because of additional gravity loads compared to the other configurations.

Global and local confirmation of the effectiveness of the seismic retrofitting techniques can be drawn from the base shear and interstorey drift demands to (DEX)F, respectively, whose values are less than half of those corresponding to the original frame. The efficiency of the FVDs is confirmed at the lower and intermediate levels while it is reduced in the top storey, thereby highlighting that a distribution of damping constants proportional to the storey shear represents a good design criterion. On the other hand, DEXF.Pa and DEX.Mi appear the best choice parallel to X and Y, respectively, when local and global drift ratios are considered. As expected, the top displacement target value is frequently exceeded by the building in its original condition, but it is sometimes exceeded when retrofitting with DEX.Pe, while DEXF.Pa and DEXF.Mi are always within the limits of this threshold. However, all DEXs induce amplification of the acceleration towards the upper levels of the original building, and this may represent a potential risk in the case of acceleration-sensitive nonstructural components. Torsional effects may occur when intermediate and exterior positions of FVDs are preferred in DEX.Pe, highlighting the fact that it is crucial to select the in-plan disposition of CBFs and FVDs for perpendicular configurations accurately.

ACKNOWLEDGEMENT

The present work was financed by Re.L.U.I.S. (Italian network of university laboratories of earthquake engineering), in line to the Convenzione D.P.C.-Re.L.U.I.S. 2019-2021, WP15, Code Revisions for Isolation and Dissipation.

ORCID

Fabio Mazza https://orcid.org/0000-0003-1019-1333

REFERENCES

1. Ramirez OM, Constantinou MC, Kircher CA, Whittaker AS, Johnson MW, Gomez JD, Chrysostomou CZ. Development and evaluation of simplified procedures for analysis and design of buildings with passive energy dissipation systems. - Revision 01. 2001; Technical report MCEER-00-0010.
2. Liang Z, Lee GC, Dargush GF, Song J. *Structural Damping: Application in Seismic Response Modification*. Boca Raton: CRC Press; 2012.
3. Constantinou MC, Soong TT, Dargush GF. Passive energy dissipation systems for structural design and retrofit. Chichester, MCEER Monograph No 1; 1998.
4. Christopoulos C, Filiatrault A. *Principles of Passive Supplemental Damping and Seismic Isolation*. Pavia, Italy: IUSS Press; 2006.

5. Foti D, Diaferio M, Nobile R. Dynamic behavior of new aluminum–steel energy dissipating devices. *Struct Control Health Monit*. 2013;20(7):1106-1119.
6. Caterino N, Spizzuoco M, Occhiuzzi A. Promptness and dissipative capacity of MR dampers: experimental investigations. *Struct Control Health Monit*. 2013;20(12):1424-1440.
7. Corbi I, Corbi O. Development and implementation of a control system for the dynamic mitigation of 3-D masonry structures with feedback on the drifts in the horizontal plane. *Struct Control Health Monit*. 2018;25:1-12, e2176.
8. Benavent-Climen A. An energy-based method for seismic retrofit of existing frames using hysteretic dampers. *Soil Dyn Earthq Eng*. 2011;31(10):1385-1396.
9. Lavan O, Abecassis D. Seismic behavior and design of wall-EDD-frame systems. *Front Built Environ*. 2015;1(7):1-17.
10. Impollonia N, Palmeri A. Seismic performance of buildings retrofitted with nonlinear viscous dampers and adjacent reaction towers. *Earthq Eng Struct Dyn*. 2018;47(5):1329-1351.
11. Trombetti T, Silvestri S. Added viscous dampers in shear-type structures: the effectiveness of mass proportional damping. *J Earthq Eng*. 2014;8:275-313.
12. Ajrab JJ, Pekcan G, Mander JB. Rocking wall-frame structures with supplemental tendon systems. *ASCE J Struct Eng*. 2004;130(6):895-903.
13. Toranzo LA, Restrepo JI, Mander JB, Carr AJ. Shake-table tests of confined-masonry rocking walls with supplementary hysteretic damping. *J Earthq Eng*. 2009;13(6):882-898.
14. Restrepo JI, Rahman A. Seismic performance of self-centering structural walls incorporating energy dissipators. *J Struct Eng*. 2007;133(11):1560-1570.
15. Qu Z, Wada A, Motoyui S, Sakata H, Kishiki S. Pin-supported walls for enhancing the seismic performance of building structures. *Earthq Eng Struct Dyn*. 2012;41(14):2075-2091.
16. Barbagallo F, Bosco M, Marino EM, Rossi PP. Seismic retrofitting of braced frame buildings by RC rocking walls and viscous dampers. *Earthq Eng Struct Dyn*. 2018;41:2075-2091.
17. Marriott D, Pampanin S, Bull D, Palermo A. Dynamic testing of precast, post-tensioned rocking wall systems with alternative dissipating solutions. *Bull New Zeland Soc Earthq Eng*. 2008;41(2):90-103.
18. Blebo FC, Roke DA. Seismic-resistant self-centering rocking core system. *Eng Struct*. 2015;101:193-204.
19. Gioiella L, Tubaldi E, Gara F, Dezi L, Dall'Asta A. Modal properties and seismic behaviour of buildings equipped with external dissipative pinned rocking braced frames. *Eng Struct*. 2018;172:807-819.
20. Makris N, Aghagholizadeh M. The dynamics of an elastic structure coupled with a rocking wall. *Earthq Eng Struct Dyn*. 2016;46(6):945-962.
21. Grigorian M, Grigorian C. An introduction to the structural design of rocking wall-frames with a view to collapse prevention, self-alignment and repairability. *Struct Design Tall Spec Build*. 2015;25:93-111.
22. ASCE 7-16. Minimum design loads for buildings and other structures. American Society of Civil Engineers; 2013. 10.1061/9780784412916.
23. Mora C, Garza O, Hernandez R. Seismic retrofit of a steel moment frame California hospital building using exterior viscous damped frames. *Structures Congress*. 2012;1:1620-1636.
24. Marini A, Passoni C, Belleri A, et al. Combining seismic retrofit with energy refurbishment for the sustainable renovation of RC buildings: a proof of concept. *Eur J Environ Civ Eng*. 2017;1-21.
25. Reggio A, Restuccia L, Martelli L, Ferro GA. Seismic performance of exoskeleton structures. *Eng Struct*. 2019;198:1-11, 109459.
26. Di Lorenzo G, Colacurcio E, Di Filippo A, Formisano A, Massimilla A, Landolfo R. State-of-the-art on steel exoskeletons for seismic retrofit of existing RC buildings. *Ingegneria Sismica*. 2020;37(1):33-50.
27. Caverzan A, Lamperti Tornaghi M, Negro P (editors). Proceedings of SAFESUST Workshop. A roadmap for the improvement of earthquake resistance and eco-efficiency of existing buildings and cities. JRC, Ispra, November 26–27, 2015.
28. Kitayama S, Constantinou MC. Seismic performance of buildings with viscous damping systems designed by the procedures of ASCE/SEI 7–16. *ASCE J Struct Eng*. 2018;144(6):1-14, 1943-541x.0002048
29. De Domenico D, Ricciardi G, Takewaki I. Design strategies of viscous dampers for seismic protection of building structures: a review. *Soil Dyn Earthq Eng*. 2019;118:144-165.
30. Pekcan G, Mander JB, Chen SS. Design and retrofit methodology for building structures with supplemental energy dissipating systems. Report No. MCEER-99-0021. New York at Buffalo; 1999.
31. Ricci P, Manfredi V, Noto F, Terrenzi M, De Risi MT, Di Domenico M, Camata G, Franchin P, Masi A, Mollaioli F, Spacone E, Verderame GM. RINTC-E: towards seismic risk assessment of existing residential reinforced concrete buildings in Italy. COMPDYN 2019, Crete, Greece; 2019.
32. McKenna F, Fenves GL, Scott MH. *Open System for Earthquake Engineering Simulation*. Berkeley, CA: University of California; 2000.
33. Ibarra LF, Medina RA, Krawinkler H. Hysteretic models that incorporate strength and stiffness deterioration. *Earthq Eng Struct Dyn*. 2005;34(12):1489-1511.
34. Mazza F. Modelling and nonlinear static analysis of reinforced concrete framed buildings irregular in plan. *Eng Struct*. 2014;80:98-108.
35. Alath S, Kunnath SK. *Modeling inelastic Shear Deformation in RC Beam-Column Joints. Proceedings of the 10th; Conference in Engineering Mechanics*. Boulder, Colorado: University of Colorado at; 1995.

36. Mazza F. Shear modelling of the beam-column joint in the nonlinear static analysis of r.c. framed structures retrofitted with damped braces. *Bull Earthq Eng*. 2018;108:111-129.
37. Mazza F. A plastic-damage hysteretic model to reproduce strength stiffness degradation. *Bull Earthq Eng*. 2019;17(6):2787-2819.
38. Mazza F. A simplified retrofitting method based on seismic damage of a SDOF system equivalent to a damped braced building. *Eng Struct*. 2019;200:1-19, 109712.
39. Terenzi G, Costoli I, Sorace S. Activation control extension of a design method of fluid viscous dissipative bracing systems. *Bull Earthq Eng*. 2020;18(8):4017-4038.
40. Silvestri S, Gasparini G, Trombetti T. A five-step procedure for the dimensioning of viscous dampers to be inserted in building structures. *J Earthq Eng*. 2010;14(3):417-447.
41. Fajfar P. A nonlinear analysis method for performance based seismic design. *Earthq Spectra*. 2000;16(3):573-592.
42. Dwairi HM, Kowalsky MJ, Nau JM. Equivalent damping in support of direct displacement-based design. *J Earthq Eng*. 2007;11(4):512-530.
43. Lin Y-Y, Chang K-C, Chen C-Y. Direct displacement-based design for seismic retrofit of existing buildings using nonlinear viscous dampers. *Bull Earthq Eng*. 2008;6(3):535-552.
44. Mazza F, Mazza M, Vulcano A. Displacement-based seismic design of hysteretic damped braces for retrofitting in-elevation irregular r.c. framed structures. *Soil Dyn Earthq Eng*. 2015;69:115-124.
45. D'Aniello CS, Landolfo R. The influence of beam stiffness on seismic response of chevron concentric bracings. *J Constr Steel Res*. 2015;112:305-324.
46. Sigaher AN, Constantinou MC. Scissor-jack-damper energy dissipation system. *Earthq Spectra*. 2003;19(1):133-158.
47. Losanno D, Spizzuoco M, Serino G. Design and retrofit of multi-story frames with elastic-deformable viscous damping braces. *J Earthq Eng*. 2017;23(9):1441-1464.
48. Fu Y, Kasai K. Comparative study of frames using viscoelastic and viscous dampers. *J Struct Eng*. 1998;124(5):513-522.
49. Hwang J-S, Lin W-C, Wu N-J. Comparison of distribution methods for viscous damping coefficients to buildings. *Struct Infrastruct Eng*. 2013;9(1):28-41.
50. Italian Building Code 86. Norme tecniche relative alle costruzioni antisismiche. DM 24–01-1986, Italian Ministry of Public Works, Rome, Italy.
51. Italian Building Code 92. Norme tecniche per le opere in c.a. normale e precompresso e per le strutture metalliche. DM 14–02-1992, Italian Ministry of Public Works, Rome, Italy.
52. Italian Building Code 18. Norme tecniche per le costruzioni. DM 17-01-2018, Italian Ministry of Infrastructures and Transports, Rome, Italy.
53. Luzi L, Hailemikael S, Bindi D, Pacor F, Mele F, Sabetta F. ITACA (ITalian ACcelerometric Archive): a web portal for the dissemination of Italian strong-motion data. *Seismol Res Lett*. 2008;79(5):716-722.
54. Ancheta TD, Darragh RB, Stewart JP, et al. NGA-West2 database. *Earthq Spectra*. 2014;30(3):989-1005.
55. Iervolino I, Spillatura A, Bazzurro P. Seismic structural reliability of code-conforming Italian buildings. *J Earthq Eng*. 201810.1080/13632469.2018.1540372;22(sup2):5-27.
56. Ghobarah A. On drift limits associated with different damage levels. In: Proceedings of the international workshop on the performance-based seismic design: concepts and implementation, Bled, Slovenia, 2004; 1:321–332.

How to cite this article: Mazza F. Dissipative steel exoskeletons for the seismic control of reinforced concrete framed buildings. *Struct Control Health Monit*. 2020;e2683. https://doi.org/10.1002/stc.2683